Disease Association of Anti–Carboxyethyl Lysine Autoantibodies in Hidradenitis Suppurativa

JIDOpen

Giulio Macchiarella[1,2], Vanessa Cornacchione[3], Celine Cojean[4], Julia Riker[4], Yichen Wang[4], Helene Te[4], Melanie Ceci[4], Johann E. Gudjonsson[5], Swann Gaulis[4], Jean François Goetschy[4], Audrey Wollschlegel[4], Stephanie K. Gass[6], Sofia Oetliker-Contin[6], Barbara Wettstein-Ling[6], Dirk J. Schaefer[6], Pascale Meschberger[7], Roland de Roche[8], Rik Osinga[6,8], Grazyna Wieczorek[4], Ulrike Naumann[9], Joachim C.U. Lehmann[4], Anna Schubart[4], Andreas Hofmann[10], Lukas Roth[4], Edwin F. Florencia[11], Christian Loesche[12], Elisabetta Traggiai[3], Alexandre Avrameas[1], Errol P. Prens[11], Till A. Röhn[4,13] and Ben Roediger[4,13]

Hidradenitis suppurativa (HS) is a chronic inflammatory skin disease characterized by recurring suppurating lesions of the intertriginous areas, resulting in a substantial impact on patients' QOL. HS pathogenesis remains poorly understood. An autoimmune component has been proposed, but disease-specific autoantibodies, autoantigens, or autoreactive T cells have yet to be described. In this study, we identify a high prevalence of IgM, IgG, and IgA antibodies directed against Nε-carboxyethyl lysine (CEL), a methylglyoxal-induced advanced glycation end-product, in the sera of patients with HS. Titers of anti-CEL IgG and IgA antibodies were highly elevated in HS compared with those in healthy controls and individuals with other inflammatory skin diseases. Strikingly, the majority of anti-CEL IgG was of the IgG2 subclass and correlated independently with both disease severity and duration. Both CEL and anti-CEL–producing plasmablasts could be isolated directly from HS skin lesions, further confirming the disease relevance of this autoimmune response. Our data point to an aberration of the methylglyoxal pathway in HS and support an autoimmune axis in the pathogenesis of this debilitating disease.

Journal of Investigative Dermatology (2022) ■, ■–■; doi:10.1016/j.jid.2022.08.051

INTRODUCTION

Hidradenitis suppurativa (HS) is a chronic inflammatory skin disease characterized by painful and recurrent nodules and abscesses, primarily affecting inverse body regions (Prens and Deckers, 2015). HS pathogenesis is clinically well-characterized, but its etiology remains poorly understood.

The association with inflammasome components, particularly IL-1β, has led to the growing consensus that HS is, at least in part, an autoinflammatory disease. The prominence of neutrophils in HS lesions, the association of HS with monogenic autoinflammatory syndromes (Figueras-Nart et al., 2019), and the responsiveness of patients with HS to anti-TNF antibodies and the IL-1 receptor antagonist contribute to this hypothesis (Savage et al., 2019; Tzanetakou et al., 2016). More recently, the possibility that HS also comprises an autoimmune (adaptive) component has emerged (Constantinou et al., 2019). The prominence of T cells, B cells, and plasma cells within HS lesions (Byrd et al., 2019; Gudjonsson et al., 2020; Musilova et al., 2020), together with emerging evidence that IL-17 inhibition may be beneficial in patients with HS (Fletcher et al., 2020), support the notion of adaptive immune cell involvement in this disease. HS has also been associated with other autoimmune diseases, particularly Crohn's disease, ulcerative colitis (UC), and spondyloarthropathies (Chen and Chi, 2019; Richette et al., 2014). Nevertheless, the role of the adaptive immune system in HS remains unclear.

Autoantibodies are a common feature in several autoimmune diseases, and their detection is used for a wide range of clinical applications, including for diagnostic and prognostic

[1]*Biomarker Development (BMD), Novartis Institutes for BioMedical Research, Novartis Pharma AG, Basel, Switzerland;* [2]*Biozentrum, Faculty of Sciences, University of Basel, Basel, Switzerland;* [3]*NIBR Biologics Center (NBC), Novartis Institutes for BioMedical Research, Novartis Pharma AG, Basel, Switzerland;* [4]*Autoimmunity, Transplantation and Inflammation (ATI) Disease Area, Novartis Institutes for BioMedical Research, Novartis Pharma AG, Basel, Switzerland;* [5]*Department of Dermatology, University of Michigan, Ann Arbor, Michigan, USA;* [6]*Department of Plastic, Reconstructive & Aesthetic Surgery and Hand Surgery, University Hospital, University of Basel, Switzerland;* [7]*Department of Surgery, Kantonsspital Baselland, Liestal, Switzerland;* [8]*Praxis beim Merian Iselin, Basel, Switzerland;* [9]*Chemical Biology and Therapeutics (CBT), Novartis Institutes for BioMedical Research, Novartis Pharma AG, Basel, Switzerland;* [10]*Biotherapeutic and Analytical Technologies, Novartis Institutes for BioMedical Research, Novartis Pharma AG, Basel, Switzerland;* [11]*Department of Dermatology, Erasmus University Medical Centre, Rotterdam, the Netherlands; and* [12]*Translational Medicine, Novartis Institutes for BioMedical Research, Novartis Pharma AG, Basel, Switzerland*

[13]*These authors contributed equally to this work.*

Correspondence: Ben Roediger, Autoimmunity, Transplantation & Inflammation Disease Area, Novartis Institutes for BioMedical Research, Basel CH-4056, Switzerland. E-mail: ben.roediger@novartis.com

Abbreviations: CEL, carboxyethyl lysine; CML, carboxy-methyl-lysine; HS, hidradenitis suppurativa; UC, ulcerative colitis

Received 9 March 2022; revised 1 August 2022; accepted 5 August 2022; accepted manuscript published online XXX; corrected proof published online XXX

purposes as well as for monitoring disease progression and treatment response. The target antigens of autoantibodies also provide insights into the underlying mechanisms of disease pathogenesis. These may include organ-specific self-proteins, for example, thyroid peroxidase in Hashimoto's disease, but also chemically modified antigens, such as deamidated peptides in coeliac disease and citrullinated peptides in rheumatoid arthritis. Elevated titers of antibodies against nuclear antigens and citrullinated peptides have also been observed in HS (Byrd et al., 2019; Mulani et al., 2018). However, to date, no disease-specific autoantigens have been identified in HS.

The metabolite methylglyoxal is produced nonenzymatically during glycolysis, specifically from glyceraldehyde-3-phosphate and dihydroxyacetone phosphate. Because methylglyoxal has cytotoxic activity, it is usually inactivated by the glyoxalase system. However, when produced in excess, methylglyoxal acts as a major precursor in the formation of advanced glycation end-products, pathogenic and proinflammatory modifications of proteins and lipids (Vistoli et al., 2013). Although methylglyoxal is produced as part of normal cellular metabolism, its production is elevated in metabolic and inflammatory diseases.

In this study, we identify antibodies against Nε-carboxyethyl lysine (CEL), a stable adduct generated by methylglyoxal, as highly prevalent and highly abundant in patients with HS. Anti-CEL IgG and IgA autoantibodies were specifically elevated in HS compared with those in healthy volunteers and individuals suffering from other inflammatory skin and autoimmune diseases, and anti-CEL IgG titers independently correlated with HS disease severity and duration. Our data lend support for an autoimmune etiology in HS and provide, to the best of our knowledge, several unreported avenues for future investigation into the pathogenesis, assessment, and treatment of this debilitating disease.

RESULTS

To identify potential autoantibodies in HS, sera from 61 patients (Hurley stages 2−3) and 22 healthy volunteers (cohort 1) were screened for the presence of autoreactive IgG, IgA, and IgM against a custom panel of 51 antigens (Figure 1a), comprising endogenous, nuclear, and microbial antigens commonly associated with inflammatory and autoimmune disease (Supplementary Table S1). The panel also included a selection of commercially available, post-translationally modified BSA, namely carboxymethyl-lysine (CML), CEL, and carbamyl-lysine, along with glycolaldehyde- and malondialdehyde-modified BSA. Of all 51 antigens assessed, only CEL showed differential Ig reactivity compared with those in healthy volunteers, particularly of the IgG and IgA isotypes (Figure 1a and b and Supplementary Figure S1a and b). Anti-CEL IgM was also significantly elevated in HS sera, but the fold change was less pronounced owing to the presence of high titers of anti-CEL IgM in healthy individuals (Supplementary Figure S1c). The fold difference in anti-CEL IgG between HS and healthy control was both substantial (9.4-fold) and robust, with ∼90% of patients with HS exhibiting greater titers than the average titer of the healthy donors (Figure 1c).

We applied receiver operating characteristic curves to evaluate the capability of anti-CEL IgG to distinguish HS sera from healthy sera, using the standard area under the curve as readout, in which a perfect classifier has an area under the curve of 1, and a random classifier gives a value of 0.5 (Søreide, 2009). Anti-CEL IgG gave an area under the curve of 0.9136 ($P < 0.0001$), which increased to 0.9367 when anti-CEL IgA was included in the classification (Figure 1d and Supplementary Figure S1d).

To assess whether anti-CEL autoantibodies are present in other inflammatory skin or autoimmune diseases, we assessed anti-CEL Ig in the sera of patients with atopic dermatitis (n = 30), acne (n = 31), UC (n = 25), and Crohn's disease (n = 13). Acne was chosen as a common comorbidity of HS (Hua et al., 2021), which has been associated with plasma cell infiltration into the skin (Carlavan et al., 2018), whereas AD is an unrelated inflammatory skin disease that nevertheless accompanies lymphadenopathy (Spergel and Paller, 2003) and changes in the B cell compartment (Czarnowicki et al., 2016). Anti-CEL titers were not significantly upregulated in acne or atopic dermatitis, although intermediate levels of anti-CEL IgG antibodies were observed in Crohn's disease and UC (Figure 1e). We conclude that anti-CEL IgG is highly prevalent and highly elevated in patients with HS.

Next, we sought to understand the relevance of CEL in HS. Carboxylethyl modifications to lysine are one of many types of advanced glycation end-products, which are collectively associated with several physiological but also pathological processes. Several other advanced glycation end-product–modified antigens were included in our original autoantibody screen, the most chemically similar to CEL being CML (Figure 2a), which elicited a modest but statistically insignificant binding in some HS sera (Figure 1a and Supplementary Figure S1a−c). We therefore assessed the specificity of the anti-CEL autoantibodies in HS in contrast to that of CML as well as octopine, a carboxylethyl modification of arginine (Figure 2a). Preincubation of HS sera with CML and octopine had minimal effect on CEL binding (Figure 2b), indicating that the autoantibodies in HS sera are specific for CEL, not CML, nor a nonlysine-associated carboxyethyl motif.

CEL but not CML is typically formed by the metabolite methylglyoxal, a glycolytic by-product that reacts with specific amino acid residues through the Maillard reaction to form stable adducts. We therefore tested the capability of methylglyoxal to induce changes to histone that might render it reactive to HS sera. We chose histone not only because of its susceptibility to methylglyoxal but also because methylglyoxal-induced post-translational adductions to histones are common in cellular metabolism (Galligan et al., 2018) and therefore represent a potential endogenous target. Recombinant human histone A2 was chemically modified by incubation with pyruvate and cyanoborohydride and was then assessed for HS sera binding by Luminex. As shown in Figure 2c, HS sera bound to modified but not unmodified histone. Because methylglyoxal can also induce modifications to arginine, particularly in histones, we also assessed the CEL specificity of this reaction by preincubating the sera in CEL. CEL preincubation completely abrogated HS

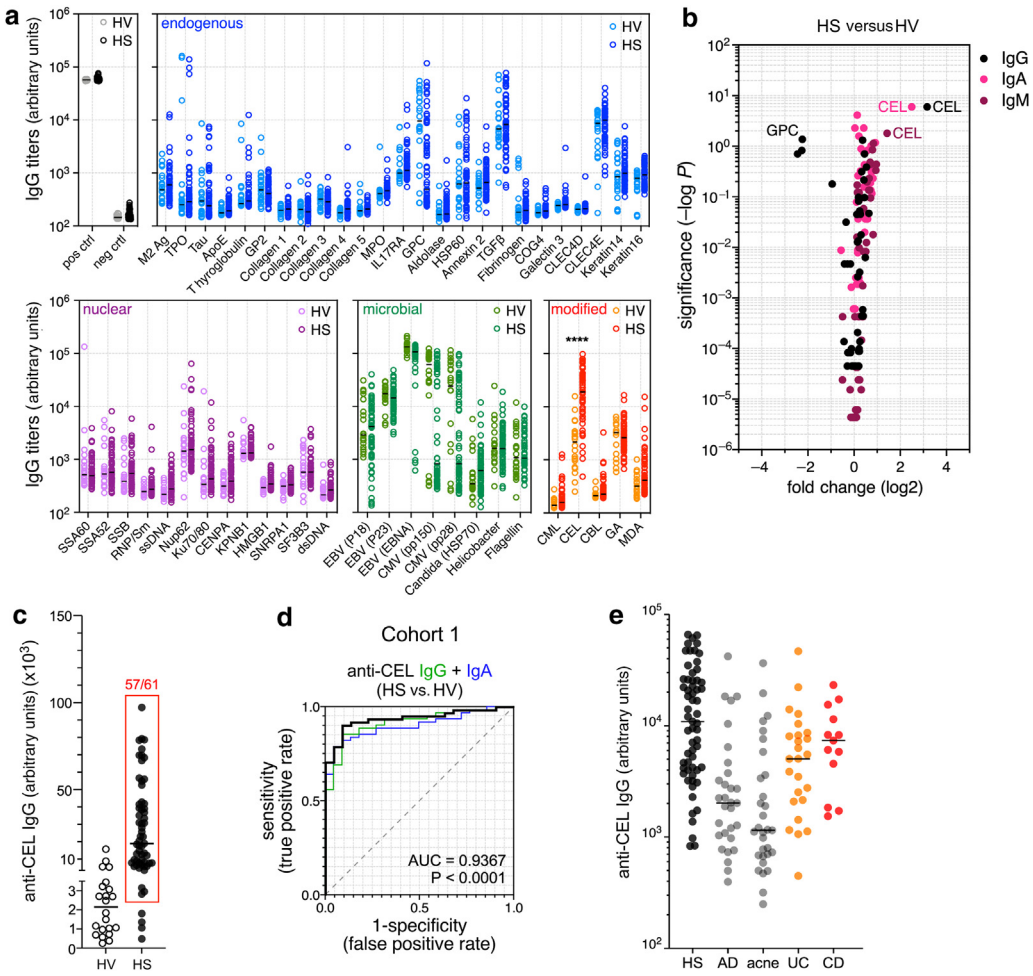

Figure 1. Identification of anti-CEL autoantibodies in HS sera. (**a**) Distribution of log-normalized titers of IgG antibodies (arbitrary units) detected in the sera of patients with HS (n = 61; cohort 1) and HV (n = 22) targeting indicated antigens, subdivided in five groups: negative/positive controls (gray/black), endogenous antigens (blue), nuclear antigens (pink/purple), microbial antigens (green), and post-translational modifications (orange/red). See Supplementary Table S1 for abbreviations. ****$P < 0.0001$ (students *t*-test). (**b**) Volcano plot depicting fold change in autoantibody titers in HS (n = 61) versus healthy (n = 22) sera; black for IgG, purple for IgM, and pink for IgA. Each dot represents a single antigen shown in **a**. Significance was calculated by *t*-test (Bonferroni corrected). (**c**) Linear scale titers of IgG anti-CEL antibodies (arbitrary units) in HS (n = 61) versus healthy (n = 22) sera. The red box identifies the number of HS samples with titers higher than the average of healthy values. (**d**) Receiver operator characteristic analysis distinguishing patients with HS from HVs on the basis of IgG (green), IgA (blue), and IgG + IgA (black) anti-CEL titers. AUC for IgG + IgA is shown. (**e**) Log distribution of IgG anti-CEL titers (arbitrary units) in serum samples from patients with indicated conditions. HS, n = 61; AD, n = 30; acne vulgaris, n = 31; CD, n = 13. UC, n = 25. AD, atopic dermatitis; ApoE, apolipoprotein E; AUC, area under the curve; CD, Crohn's disease; CEL, carboxyethyl lysine; dsDNA, doule-stranded DNA; EBV, Epstein-Barr virus; GA, Glycoaldehyde; GPC, gastric parietal cell antigen; HS, hidradenitis suppurativa; HV, healthy volunteers; MDA, malondialdehyde; MPO, myeloperoxidase; neg ctrl, negative control; pos ctrl, positive control; ssDNA, single-stranded DNA; TPO, thyroid peroxidase; UC, ulcerative colitis.

sera reactivity to methylglyoxal-modified histone (Figure 2d). These data strongly imply that anti-CEL autoantibodies bind to CEL independently of the modified protein.

We then sought to detect CEL directly in healthy and HS lesional skin. Resected tissue from patients with Hurley stages 2 and 3 (n = 12) undergoing surgery were biopsied, and the tissue was snap frozen and lysed before assessment for and quantification of CEL by simple ELISA. Nonlesional as well as healthy donor skin was included as controls. CEL was detected in all samples, but in 3 of 12 lesional samples, CEL was especially abundant, ~3-fold greater than in control samples (Figure 2e). We conclude that autoantibodies against CEL in HS are highly CEL specific and that CEL modifications are likely present in healthy skin and may be abundant in some HS lesions.

To understand the clinical relevance of anti-CEL autoantibodies in HS, we repeated these measurements in plasma samples from a second, clinically well-validated cohort of 40 patients with HS (cohort 2), which included patients across the entire severity spectrum (i.e., Hurley stages 1–3) and in which additional clinical data, including refined Hurley score and age of onset, were known. Patient characteristics for both cohorts are summarized in Supplementary Table S2. We confirmed the high titers of anti-CEL IgG and IgA in patients with HS in cohort 2 (Figure 3a and b and data not shown), although the magnitude of the effect was smaller in the second cohort (3.85-fold), possibly owing to increased variability of control plasma compared with that of serum. The receiver operating characteristic curve comparing anti-CEL in HS with that in healthy plasma gave an area under

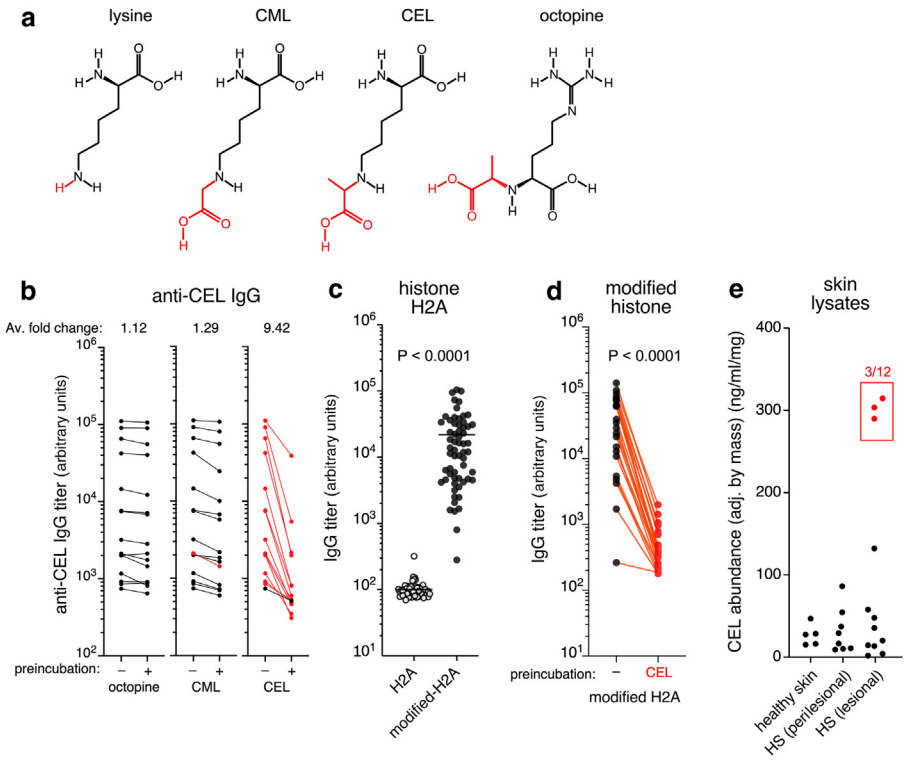

Figure 2. Specificity of anti-CEL autoantibodies in HS sera. (**a**) Chemical structures of lysine, CML, CEL, and octopine. (**b**) Titers (arbitrary units) of IgG anti-CEL in HS plasma samples (n = 15) with and without preincubation with octopine, CML, or CEL. Data points connected by a line belong to the same patient. Red connections represent a decrease of greater than 1.5-fold in anti-CEL BSA signal after sample preincubation. (**c, d**) Titers of IgG against recombinant human histone A2 and histone that was chemically modified by incubation with pyruvate and cyanoborohydride in HS serum samples (n = 61) (**c**) without or (**d**) after preincubation with CEL. Data points connected by a line belong to the same patient. ****$P < 0.0001$ (Man–Whitney U test). (**e**) Levels of CEL detected in healthy (n = 5), perilesional HS (n = 8), and lesional HS (n = 12) skin by direct ELISA. The red box identifies 3 of 12 lesional HS samples, with CEL levels markedly higher than those of healthy skin. Av, average; CEL, carboxyethyl lysine; CML, carboxy-methyl-lysine; HS, hidradenitis suppurativa.

the curve of 0.7037 ($P = 0.0027$) for IgG, which increased to 0.7404 when anti-CEL IgA was included in the classification (Figure 3c and Supplementary Figure S2a). Importantly, these data enabled us to perform correlation analyses of anti-CEL against relevant clinical parameters.

We did not observe any relationship between anti-CEL IgG titer and sex, body mass index, smoking status, or age in either cohort (data not shown). In contrast, we observed a weak correlation between anti-CEL IgG titers and disease severity (refined Hurley stage) (r = 0.3173, $P = 0.0461$) and a stronger correlation with disease duration (r = 0.3528, $P = 0.0114$) in cohort 2 (Figure 3d and e). We did not observe a correlation between disease duration and disease severity in cohort 2 (Figure 3f), consistent with previous reports indicating that patients with HS generally reach their maximum disease activity shortly after disease onset, after which their status remains relatively stable (Kromann et al., 2014; Vanlaerhoven et al., 2018; von der Werth and Williams, 2000). Thus, anti-CEL IgG titers appeared to independently correlate with disease severity and duration. When we binned patients into five disease-severity subgroups, anti-CEL IgG titers were lowest in patients with mild, recently acquired disease and highest in patients with severe, long-lasting disease (Figure 3g). Consistent with this, we saw a good correlation between anti-CEL IgG and a combination of severity and duration (r = 0.4550, $P = 0.0012$) (Figure 3h and Supplementary Figure S2a–f and see Materials and Methods for details). Interestingly, anti-CEL IgA titers did not correlate with severity, disease duration, or the combination of the two (Figure 3i and data not shown). Similarly, anti-CEL IgM titers did not correlate with severity, disease duration, or the combination, but interestingly, anti-CEL IgM titers were lower in patients treated with antibiotics (Supplementary Figure S2g and h). We conclude that anti-CEL IgG but not anti-CEL IgA or IgM independently correlates with disease severity and duration in patients with HS.

Several groups have identified the presence of B cells and plasma cells within affected skin of patients with HS, with one study suggesting the existence of pseudo lymphoid follicles (van der Zee et al., 2012). This raised the possibility that the anti-CEL autoantibodies were being generated within the skin. To assess this potentiality, we first confirmed the presence of B cells in HS lesions by immunostaining for the B cell–specific marker CD20. B cells were present in all tissues examined, where they were either loosely organized in the dermis in association with abscesses or tunnels (Figure 4a and Supplementary Figure S3a) or more tightly ordered in smaller lymphoid clusters, many of which were associated with $CD21^+$ follicular dendritic cells, indicative of germinal center–like structures (Figure 4b). Many follicular-type clusters were observed adjacent to subcutaneous adipose tissue (Figure 4c–e), which are relevant because adipocytes have been implicated in tertiary lymphoid organ formation in Crohn's disease (Guedj et al., 2019). Spatial RNA profiling of

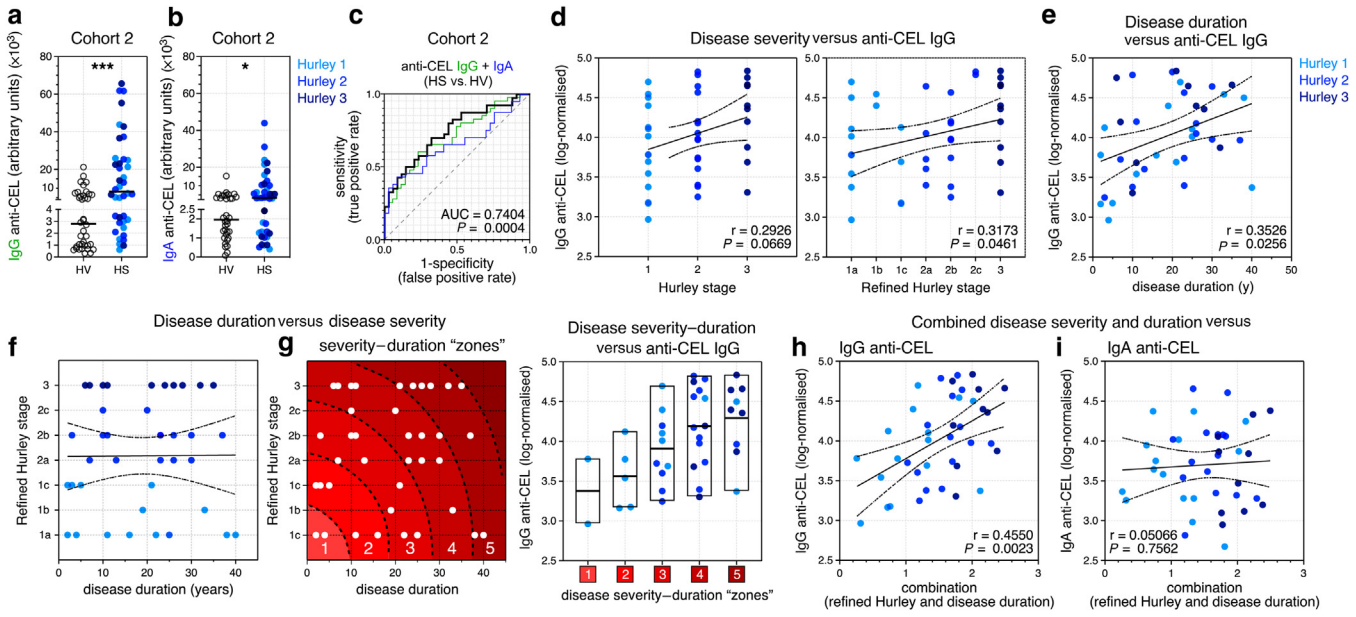

Figure 3. Anti-CEL IgG correlates with disease duration and severity in patients with HS. (**a, b**) Linear distribution of (**a**) IgG and (**b**) IgA anti-CEL titers in plasma samples of healthy volunteers (n=38) and HS patients (n = 40; cohort 2). ***$P = 0.0001$ (IgG) and *$P = 0.0265$ (IgA) (Man–Whitney *U* test). (**c**) Receiver operator characteristic analysis distinguishing patients with HS (n = 40) from healthy volunteers (n = 38) on the basis of IgG (green), IgA (blue), and IgG + IgA (black) anti-CEL titers. AUC for IgG + IgA is shown. (**d**) Scatter plot depicting the modest positive correlation between log-normalized IgG anti-CEL titers in HS plasma samples from cohort 2 (n = 40) versus Hurley score (left) and refined Hurley score (right) (Spearman test). (**e**) Scatter plot showing the positive correlation between log-normalized IgG anti-CEL titers in HS plasma samples and disease duration ($P = 0.0256$; Spearman test). (**f**) Scatter plot showing the lack of correlation between disease duration and refined Hurley score in patients with HS ($P = 0.7628$; Spearman test). (**g**) Left: Demarcation of disease duration–severity zones based on refined Hurley score and disease duration (see also Supplementary Figure S2). Right: Log-normalized IgG anti-CEL titers in indicated HS groups. (**h**) Scatter plot showing the positive correlation between log-normalized IgG anti-CEL titers in HS plasma samples and a linear combination (Euclidean distance) of refined Hurley score and disease duration ($P = 0.0023$; Spearman test). (**i**) Scatter plot showing the lack of correlation between log-normalized IgA anti-CEL titers in HS plasma samples and a linear combination of refined Hurley score and disease duration ($P = 0.7562$; Spearman test). AUC, area under the curve; CEL, carboxyethyl lysine; HS, hidradenitis suppurativa.

HS sections comparing diffuse regions of B cells with follicular-type clusters confirmed the enrichment of germinal center–associated transcripts, including *C3*, *CR2* (encoding CD21), and *FDCSP* (Figure 4f–h and Supplementary Figure S3b and c and Supplementary Table S3), although other germinal center–associated transcripts, including *AICDA* and *IL21*, were not readily detected on this platform. Finally, a retrospective analysis of our previously published transcriptomics data (Penno et al., 2020) confirmed the association between B cell–associated transcripts and lesional but not nonlesional tissue (Figure 4i), where we also observed an association between *CR2* expression and *CXCL13*, *FDCSP*, and *CR1* (encoding CD35) (Figure 4j), markers of follicular dendritic cells. We conclude that B cells are prominent in HS lesional tissue and that some but not all HS lesions contain ectopic germinal centers and follicular dendritic cells.

To verify the presence of plasma cells in HS lesions, we used flow cytometry. Resected tissue from patients with Hurley stages 2–3 (n = 7) was subjected to enzymatic digestion, single cell isolation, and subsequent antibody staining and assessment by flow cytometry. (Non-naïve) B cells were identified as $CD45^+$ $CD19^+$ IgD^- $CD20^{hi}$ $HLA\text{-}DR^+$ cells, whereas plasmablasts were identified as $CD19^+$ $CD20^{lo}$ $CD38^{hi}$. Bona fide plasma cells were identified on the basis of CD27 expression within the $CD38^{hi}$ plasmablast population (Figure 5a). In these experiments, we also included CD86, a B cell activation marker, and CD63, which we identified as a plasma cell–enriched surface molecule in a single-cell RNA-sequencing dataset from HS skin (Supplementary Figure S4a and b). Both B cells and plasmablasts were abundant in lesional HS skin, consistent with previous studies. Of note, we also observed CD86 expression by a subpopulation of B cells and a transitory $CD63^+$ population bridging the B cells to the plasma cells (Figure 5a–d), suggestive of in situ differentiation of $HLA\text{-}DR^+$ $CD63^-$ B cells into $CD63^{hi}$ $CD38^{hi}$ plasmablasts. We also observed an $HLA\text{-}DR^-$ $CD38^{hi}$ $CD63^{hi}$ $CD27^+$ population that lacked CD19 (Figure 5e), consistent with the phenotype of long-lived plasma cells (Halliley et al., 2015).

Phenotyping of these cells for surface IgG, IgM, and IgA subclasses revealed a predominance of $IgG1^+$ and $IgA1^+$ subclasses in both B cells and plasmablasts (Figure 5f and g and Supplementary Figure S4c and d). $IgG2^+$ cells were consistently observed in both subsets, albeit at a reduced frequency. $IgG3^+$ and $IgG4^+$ cells were rare, as were IgM^+ cells. Relative to B cells, IgA^+ cells were markedly reduced in plasmablasts and plasma cells (Figure 5f and g and Supplementary Figure S4e), suggesting a potential selection bias limiting IgA-producing cells from entering the plasmablast/plasma cell compartment. Collectively, we identify a spectrum of B cells, plasmablasts, and plasma cells in varying states of activation and differentiation, consistent with dynamic B cell activity within lesional HS skin.

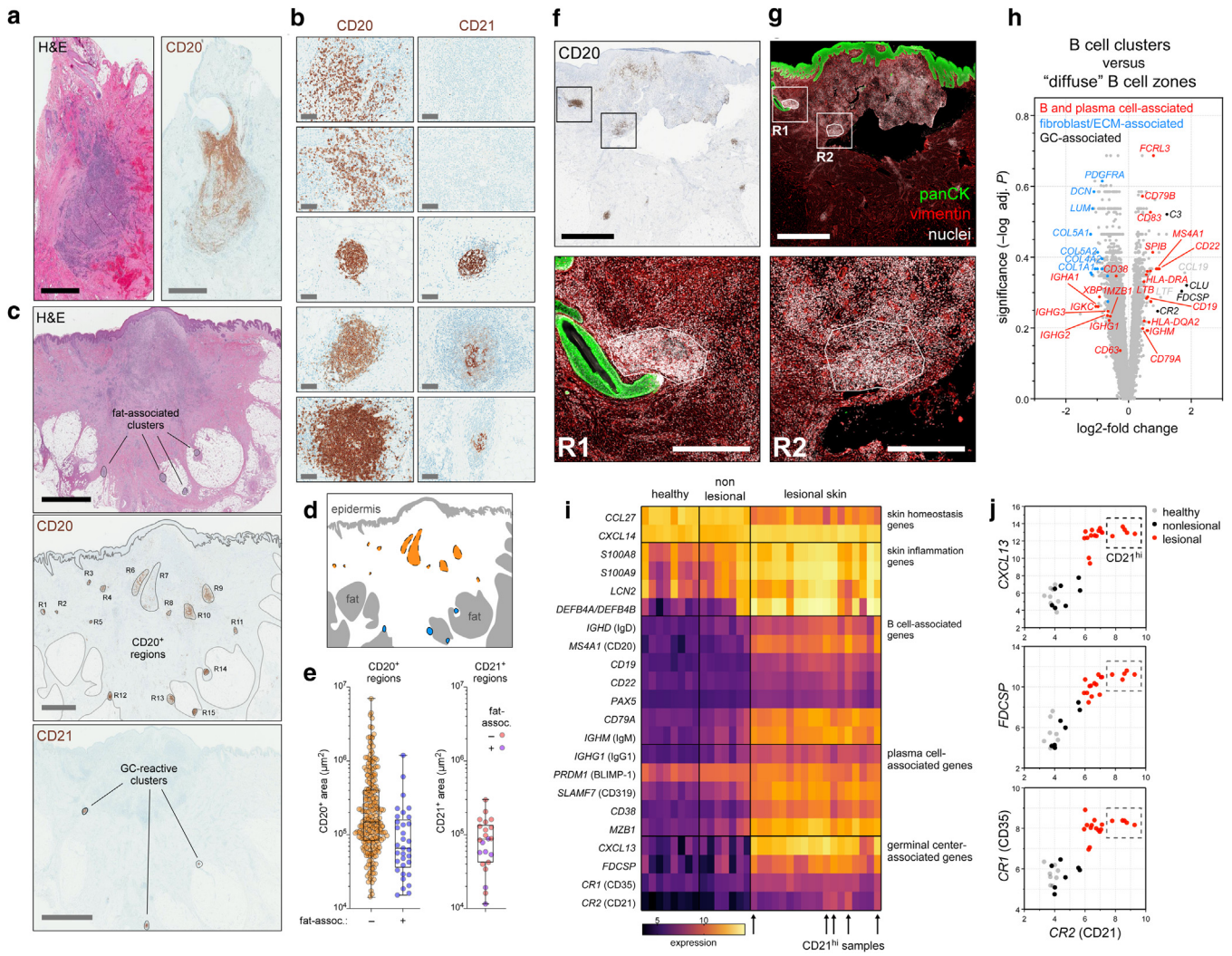

Figure 4. Detection of B cells and germinal center–like structures in HS skin. (**a**) Representative H&E (left) and CD20 staining (right) of HS skin. Each bar = 2 mm. (**b**) Representative staining of $CD20^+$ B cells (left) and $CD21^+$ germinal center–like structures (right) in HS skin. B cells were either diffusely distributed (top two panels) or densely organized in lymphoid follicles (bottom three panels), which often but not always accompanied CD21 expression. Each bar = 100 µm. (**c**) Representative H&E (top; bar = 3 mm), CD20 (middle; bar = 2 mm), and CD21 (bottom; bar = 3 mm) staining of HS skin, showing fat associated and $CD21^+$ follicles. (**d**) Schematic of **c** demarking epidermis and fat (gray) and fat-associated (blue) and non-fat–associated (orange) $CD20^+$ regions. (**e**) Quantitation $CD20^+$ (left) and $CD21^+$ (right) areas (in μm^2), stratified according to their association with fat. Collectively, these data represent 269 ROIs across 10 HS patient samples. (**f**) Representative CD20 and (**g**) immunofluorescence staining of serial sections of a skin sample of patients with HS (each bar = 2 mm), identifying a B cell cluster (R1) and a diffuse B cell zone (R2). Each bar in R1 and R2 = 0.5 mm. See also Supplementary Figure S3c. (**h**) Comparison of gene expression in B cell clusters (nine ROIs) versus diffuse B cell zones (11 ROIs) by volcano plot (n = 4 patients), as measured by NanoString Digital Spatial Profiling. Selected genes expressed by B cells and plasma cells are marked in red, fibroblast-associated genes are marked in blue, and GC-implicated genes are marked in black. See also Supplementary Table S3. (**i**) Heatmap depicting the expression of indicated genes in mRNA expression data (microarray; (Penno CA et al., 2020)) from healthy (n = 8), nonlesional HS (n = 7), and lesional HS (n = 18) skin. Arrows indicate five HS samples with an enriched expression of *CR2* (encoding CD21) in lesional skin. (**j**) Scatter plots of selected GC-associated genes from **i**. $CD21^{hi}$ samples (boxed) are associated with concomitant expression of *CR1*, *CXCL13*, and *FDCSP*. GC, germinal center; HS, hidradenitis suppurativa; PanCK, pan-cytokeratin; ROI, region of interest.

To assess the capacity of skin B cells and plasmablasts to produce anti-CEL autoantibodies, we performed enzyme-linked immunosorbent spots on sorted populations from three patients with HS in which adequate cell numbers could be obtained for such functional analyses. Specifically, $CD45^+$ $CD3^-$ $CD19^+$ IgD^- $CD20^{hi}$ $CD38^{lo}$ (non-naïve) B cells and $CD20^{lo}$ $CD38^{hi}$ plasmablasts were sorted to high purity and plated on CEL BSA–coated membranes in tissue culture media and assessed for IgG and IgA secretion the following day (Figure 5h and Supplementary Figure S5a). Global IgA and IgG secretion was also assessed and observed in both B cells and plasmablasts (Supplementary Figure S5b). CEL-specific Ig was infrequently observed from sorted B cells (Figure 5i and data not shown), but CEL-specific IgG and IgA were readily detected in plates incubated with plasmablasts sorted from all the three patients, without the need for further stimulation in vitro, a hallmark of plasmablasts/plasma cells (Figure 5j and data not shown). We conclude that anti-CEL–specific plasmablasts are present in lesional skin of patients with HS and produce anti-CEL antibodies in situ.

Finally, we were interested in the functional consequences of the anti-CEL Igs. Our initial examination of HS sera from

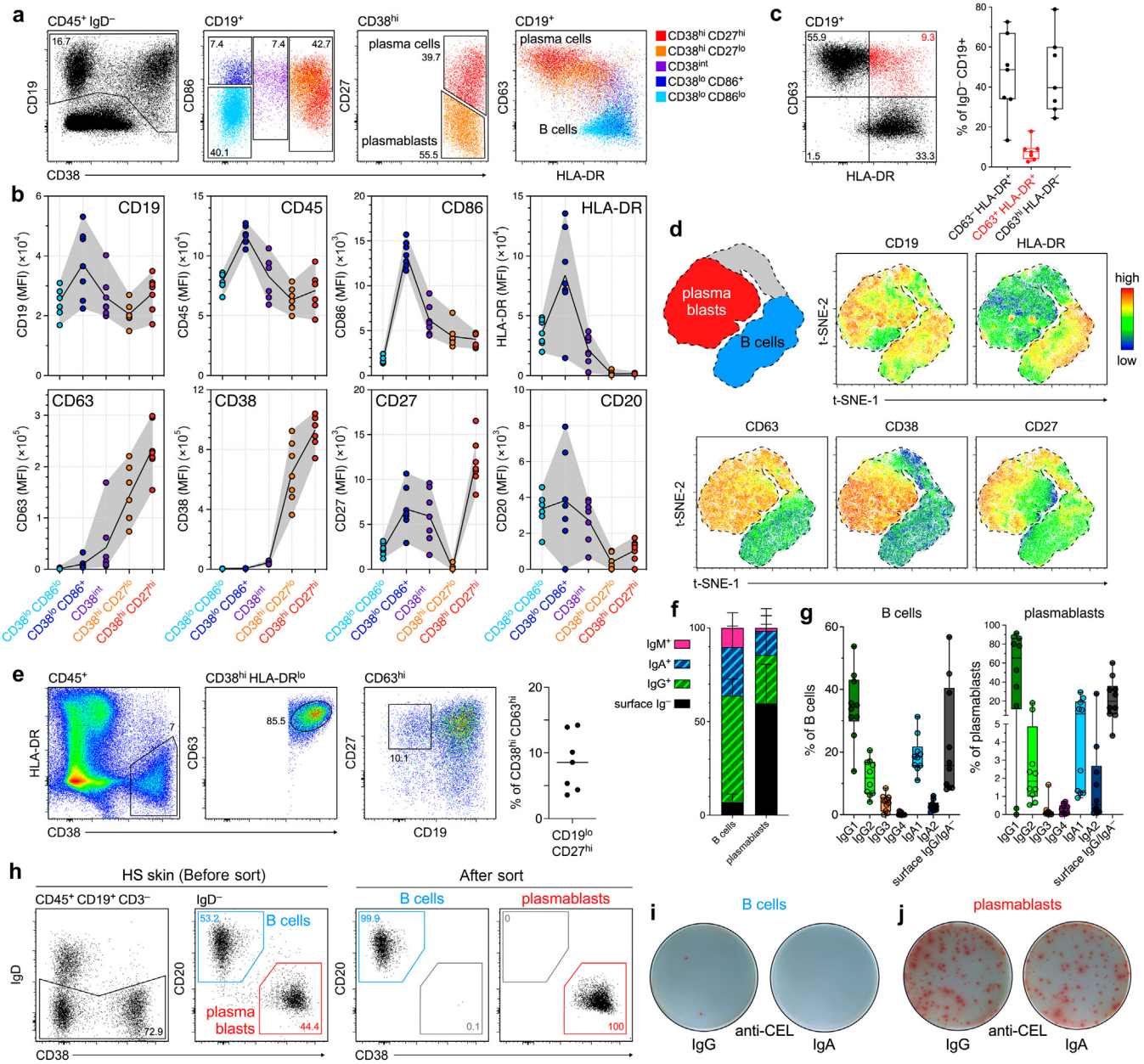

Figure 5. Detection of anti-CEL autoantibody-producing plasmablasts in HS skin. (**a**) Representative flow cytometry dotplots of (non-naïve) B cells ($CD45^+$ IgD^- $CD19^+$ $CD38^{lo}$), plasmablasts ($CD38^{hi}$), and plasma cells ($CD38^{hi}$ $CD27^+$) in lesional HS skin. (**b**) MFI values for indicated surface markers across the five B- and plasma cell populations identified in **a** (n = 7). (**c**) Representative flow cytometry dotplot (left) and frequencies (right) of HLA-DR^+ $CD63^-$ B cells, HLA-DR^- $CD63^{hi}$ plasmablasts, and HLA-DR^+ $CD63^+$ (transitional) cells (red) in lesional HS skin. (**d**) t-SNE plots of flow cytometry data from $CD19^+$ cells isolated from HS skin. Top left: Schematic defining the location of B cells (blue), plasmablasts (red), and transitional cells (gray) in the accompanying t-SNE plots. (**e**) Identification of $CD38^{hi}$ $CD63^{hi}$ $CD19^{lo}$ $CD27^+$ cells resembling long-lived plasma cells in lesional HS skin (n = 7). (**f**) The proportion of B cells and plasmablasts expressing surface IgM (pink), IgA (blue), and IgG (green) in HS skin samples (n = 7). The proportion of surface Ig^- cells is shown in black. (**g**) Proportions of B cells (left) and plasmablasts (right) expressing indicated IgG and IgA subclasses in HS skin samples (n = 10). (**h**) Representative flow cytometry dotplots of (non-naïve) $CD20^{hi}$ $CD38^{lo}$ B cells (blue) and $CD20^{lo}$ $CD38^{hi}$ plasmablasts (red) in lesional HS skin before (left) and after (right) sorting for ELISPOT readouts. (**i, j**) Representative ELISPOT plates of sorted B cells and plasmablasts (2.5×10^4 cells per well) isolated from HS skin, identifying the presence of CEL-specific antibody-secreting cells. Data are representative of three independent experiments. CEL, carboxyethyl lysine; ELISPOT, enzyme-linked immunosorbent spot; HS, hidradenitis suppurativa; MFI, mean fluorescence intensity; t-SNE, t-distributed stochastic neighbor embedding.

cohort 1 indicated the presence of anti-CEL IgM, IgG, and IgA and that all the three subclasses could compete equally for CEL binding in vitro (data not shown), but we had not identified the IgG subclasses nor performed any functional assays. We therefore reassessed the plasma samples from cohort 2 for IgG isotype specificity. Strikingly, the vast majority of anti-CEL IgG was IgG2 (Supplementary Figure S6a). Consistent with this, anti-CEL IgG2 titers correlated near perfectly with total anti-CEL IgG titers, and deviations from this correlation were explained by the presence of additional IgG1 and IgG3 subclasses in a subset of patients (Supplementary Figure S6b and c). IgG2 is typically associated with bacterial capsular

polysaccharide antigens and is weakly capable of activating complement and Fc receptor cross-linking. We assessed both in vitro, using CEL BSA as a model antigen. For complement activation, we used the plasma from cohort 2, which contained variable titers of anti-CEL IgG1, IgG2, IgG3, IgM, and IgA. Plates were coated with CEL BSA before the addition of HS or healthy control plasma, washed, and then provided excessive complement from healthy serum and incubated for 1 hour at 37 °C. Soluble C5b-9 was used as a readout of complement activation. Half of the sample of patients with HS exhibited complement activation above that seen in healthy controls (Supplementary Figure S6d). Soluble C5b-9 correlated weakly with individual anti-CEL IgG and IgM titers but very strongly with a combination of both IgG and IgM (Supplementary Figure S6e–g), suggesting that both IgG and IgM subclasses contributed to complement activation in this assay.

For the Fc receptor activation experiments, we used locally and commercially obtained serum from patients with HS, together with in vitro generated macrophages. We stimulated macrophages with a mixture of CEL BSA and HS serum, measuring TNF secretion as readout. Macrophages treated with CEL BSA alone or CEL BSA with healthy serum were negative (data not shown), whereas HS serum alone similarly induced negligible TNF secretion across the seven donors assessed (Supplementary Figure S6h). In contrast, serum from 2 of 7 donors with HS induced robust TNF production in combination with CEL BSA, which correlated with IgG2 titers (Supplementary Figure S6h and data not shown). We conclude that anti-CEL autoantibodies are capable of activating complement and macrophages in vitro.

DISCUSSION

In this study, we identify anti-CEL IgGs as highly prevalent and highly abundant autoantibodies in patients with HS. Anti-CEL–producing plasmablasts were detectable within lesional skin, and anti-CEL IgG titers correlated with both disease duration and severity of patients with HS. Although autoantibodies have been previously identified in HS, for example, antinuclear antibodies and anticyclic citrullinated peptide (Byrd et al., 2019; Carmona-Rivera et al., 2022; Mulani et al., 2018), they have all been associated more markedly with other autoimmune diseases (i.e., systemic lupus erythematosus and rheumatoid arthritis, respectively). To the best of our knowledge, this study identifies a hitherto unknown association between anti-CEL autoantibodies and HS that demonstrate a high degree of disease specificity. Nevertheless, anti-CEL IgG is not a conventional autoantibody, being mainly of the IgG2 subtype. This observation was striking and unexpected because most pathogenic antibodies are IgG1 or IgG4, whereas natural (non-IgM) autoantibodies are believed to favor the IgG3 subclass (Lobo, 2016). IgG2 plays an important role against encapsulated bacteria (Vidarsson et al., 2014), but the relevance of the anti-CEL IgG2 in HS remains unclear. Although our data do not provide a formal demonstration for a potential pathogenic role of anti-CEL autoantibodies in HS, in vitro, anti-CEL IgG could activate both complement and macrophages and is thus theoretically capable of proinflammatory functions. Alternatively, anti-CEL IgG may serve counter-inflammatory and/or protective functions, as has been theorized for other autoantibodies (Pisetsky, 2012).

A second finding around this target relates to the high titers of anti-CEL IgM antibodies in healthy subjects, which is consistent with the previously reported presence of natural autoantibodies against advanced glycation end products and other naturally occurring adducts in healthy individuals and patients with diabetes (Shibayama et al., 1999; Turk et al., 2001; Wang et al., 2013). Indeed, CEL is a common modification in mammalian physiology and is readily detectable within the serum of healthy individuals, which aligns with the function of natural autoantibodies in homeostatic maintenance. However and notably, few healthy individuals exhibited concordantly high anti-CEL IgG and rarely to the levels seen in patients with HS. Thus, it is not the presence of anti-CEL autoantibodies that appears to be disease defining but rather the conversion to IgG- and IgA-producing subclasses. How, when, and where such class switching occurs remains unknown, but we speculate on the basis of our results that the inflammatory skin lesions themselves may serve as a site of IgG and IgA plasma cell generation.

The predominance of anti-CEL IgG2 may reflect the chronic nature of HS, as might be explained by the temporal model, which predicts the emergence of IgG2 later in immune responses (Collins and Jackson, 2013). Alternatively, this may reflect qualitative features of the microenvironment during class switching, for example, the presence of IFN-γ (Kitani and Strober, 1993). It is also possible that the anti-CEL IgG2 reflects the nature of T cell help or lack thereof. The potential role of T cells in anti-CEL generation was not investigated in our study and remains an important avenue for future investigation. However, it should be noted that T-cell recognition of methyl-lysines has been recently reported (Corbière et al., 2020), raising the possibility that patients with HS may uniquely harbor T cells specific for carboxyethyl-lysine. The origins and effector functions of autoreactive CEL-specific T cells within patients with HS, presuming that they exist, remain completely unknown and require future investigation.

The selective detection of CEL- but not CML-specific autoantibodies in HS strongly implicates a role for methylglyoxal in the etiology of the disease. Dysregulation of the methylglyoxal pathway has been identified and extensively investigated in the context of type 2 diabetes and metabolic disorders (Maessen et al., 2015; Schalkwijk and Stehouwer, 2020; Shamsaldeen et al., 2016), both common comorbidities in HS. It is therefore tempting to speculate that there exists an interplay between global metabolic changes and the immune recognition of the associated protein modifications. However, the lack of association between anti-CEL titers and body mass index undermines this concept, and there exist more proximal explanations. For example, methylglyoxal is a byproduct of glycolysis, a driver of inflammation (Soto-Heredero et al., 2020). Indeed, a recent report suggests that myeloid cells utilize methylglyoxal as part of an anti-inflammatory mechanism (Baumann et al., 2020). Thus, it is likely that HS lesions are abundant in methylglyoxal, which may modify the abundance and/or distribution of CEL-modified proteins in HS lesional skin.

The relationship between anti-CEL IgG titers with both disease severity and duration is suggestive of a disease process in which CEL-reactive B cells are generated and/or expanded proportionally to disease severity and that these cells also persist for several years. On the basis of our flow cytometry and enzyme-linked immunosorbent spot experiments with HS skin, we speculate that this process involves the in situ generation of CEL-specific plasmablasts, some of which may persist into long-lived plasma cells. Increased plasma cells have been observed in the blood of patients with HS (Musilova et al., 2020), which would be consistent with the trafficking of skin-derived plasma cells to the bone marrow. An important consequence of this interpretation is the prediction that anti-CEL IgG titers can be expected to accumulate throughout life and serve as a permanent record of global disease burden. If true, anti-CEL IgG may hold important prognostic value, particularly in epidemiological studies. Anti-CEL autoantibodies may additionally hold potential as diagnostic and/or severity biomarkers in HS (Der Sarkissian et al., 2022).

Finally, the presence of anti-CEL autoantibodies in patients with Crohn's and UC (albeit at lower titers than in HS) adds to an intriguing list of commonalities between HS and inflammatory bowel disease. Inflammatory bowel disease, particularly Crohn's, but also UC is more common in patients with HS than in the general population (Chen and Chi, 2019). Both Crohn's disease and UC lesions are similarly characterized by B cell infiltrates (Defendenti et al., 2012). HS also shares other histopathological features with Crohn's, particularly the perifistular ulceration and granulomatous cutaneous inflammation (Principi et al., 2016), and all the three diseases respond to anti-TNF therapy. Together, these data suggest that methylglyoxal and anti-CEL autoantibodies may also play a role in inflammatory bowel disease and adds weight to the notion that there exist several shared pathological pathways between HS and inflammatory bowel disease.

In conclusion, our data define a hitherto unappreciated and unconventional pathway of autoantibody production in HS, which raises several questions but also opportunities for better understanding and management of this devastating disease.

MATERIALS AND METHODS

Serum and plasma samples from patients with HS

The sera of patients in cohort 1 were taken from patients with HS during their baseline visit as part of a proof-of-concept, phase 2 randomized clinical trial of CJM112, a human anti−IL-17A/IL-17AF high-affinity IgG1κ mAb in HS (NCT02421171). Only baseline samples (i.e., untreated at the time of collection) from patients who signed written informed consent for exploratory biomarker analysis were used. Patient characteristics collected as part of the study are summarized in Supplementary Table S2. The plasma of patients in cohort 2 was collected from 40 patients with HS recruited through the HS outpatient clinic of the Department of Dermatology, Erasmus University Medical Center (Rotterdam, The Netherlands). All samples were obtained with written informed consent from the participants in accordance with the Declaration of Helsinki principles, the Swiss Human Research Act, and the approval of the responsible ethics committee (Ethikkommission Nordwest- und Zentralschweiz).

HS skin samples

Skin from patients with HS undergoing surgical excision was received from the Department of Plastic, Reconstructive, Aesthetic and Hand Surgery of the University Hospital Basel (Basel, Switzerland); from the Clinic for General, Visceral, Vascular and Thoracic Surgery, Cantonal Hospital Baselland (Liestal, Switzerland); or from Praxis beim Merian Iselin (Basel, Switzerland), or the patients were recruited from the HS outpatient clinic of the Department of Dermatology, Erasmus University Medical Center. All patients provided written informed consent, and the study was conducted in accordance with the ethical principles originating in the Declaration of Helsinki and approved by the Institutional Review Board of the Erasmus University Medical Center.

Autoantibody profiling

Autoantibodies were detected using a custom-made Luminex assay on the basis of magnetic beads. All washing steps of magnetic beads in tubes and plates were performed with the support of magnetic separation plates.

Quantification and statistical analyses

The statistical details and tests used, the number and representation of n, and any other forms of quantification present are specified in the respective figure legends and results section.

Additional details of the data and approaches are available in the Supplementary Materials and Methods.

Data availability statement

The authors confirm that the data supporting the findings of this study are available within the article and its supplementary materials. Datasets related to this article can be found at https://www.ncbi.nlm.nih.gov/geo/query/acc.cgi?acc=GSE148027, hosted at the Gene Expression Omnibus, GSE148027.

ORCIDs
Giulio Macchiarella: http://orcid.org/0000-0001-9959-3675
Vanessa Cornacchione: http://orcid.org/0000-0002-4551-5193
Celine Cojean: http://orcid.org/0000-0003-2399-9833
Julia Riker: http://orcid.org/0000-0001-5024-6170
Yichen Wang: http://orcid.org/0000-0003-1955-2318
Helene Te: http://orcid.org/0000-0002-2872-2430
Melanie Ceci: http://orcid.org/0000-0003-1830-8057
Johann E. Gudjonsson: http://orcid.org/0000-0002-0080-0812
Swann Gaulis: http://orcid.org/0000-0001-8319-7723
Jean François Goetschy: http://orcid.org/0000-0002-8077-9725
Audrey Wollschlegel: http://orcid.org/0000-0002-3408-1190
Stephanie K. Gass: http://orcid.org/0000-0002-0181-161X
Sofia Oetliker-Contin: http://orcid.org/0000-0002-4419-8480
Barbara Wettstein-Ling: http://orcid.org/0000-0002-8718-7351
Dirk J. Schaefer: http://orcid.org/0000-0002-9619-8650
Pascale Meschberger: http://orcid.org/0000-0003-1871-1145
Roland de Roche: http://orcid.org/0000-0003-3001-0544
Rik Osinga: http://orcid.org/0000-0002-3333-0757
Grazyna Wieczorek: http://orcid.org/0000-0001-9212-7858
Ulrike Naumann: http://orcid.org/0000-0001-7783-7675
Joachim C.U. Lehmann: http://orcid.org/0000-0001-6554-1885
Anna Schubart: http://orcid.org/0000-0003-4253-0600
Andreas Hofmann: http://orcid.org/0000-0001-5450-6267
Lukas Roth: http://orcid.org/0000-0001-9270-1936
Edwin F. Florencia: http://orcid.org/0000-0001-9005-4464
Christian Loesche: http://orcid.org/0000-0001-6505-0349
Elisabetta Traggiai: http://orcid.org/0000-0002-0616-6285
Alexandre Avrameas: http://orcid.org/0000-0003-4094-5829
Errol P. Prens: http://orcid.org/0000-0002-8158-660X
Till A. Röhn: http://orcid.org/0000-0002-2448-3110
Ben Roediger: http://orcid.org/0000-0002-4593-091X

CONFLICT OF INTEREST

AA, AH, AS, AW, BR, CC, CL, ET, GW, HT, JCUL, JFG, JR, LR, MC, SG, TAR, UN, VC, and YW are current or former employees of and hold company stocks or stock options with Novartis Pharma AG.

ACKNOWLEDGMENTS

We thank Annette Begrich, Matthias Jecklin, Mateusz Piksa, and Paul Schroeder for the coordination of human tissue acquisition. We thank Astrid Jullion for assistance with the clinical data. We thank Friedrich Raulf, Corinne Vedrine, Elena Degl Innocenti, and Siwar Garmattou for reagents and technical assistance. We also acknowledge the flow cytometry assistance of Cyril Allard, Emeline Thevenon, Matthias Wrobel, Martine Marchant, and Elodie Riquet. We thank the team at NanoString Technologies, particularly Jennifer Hart and Jingjing Gong. We thank Georg Martiny-Baron, Feriel Hacini-Rachinel, Julian Storim, Rainer Hillenbrand, Catherine Regnier, Sandro Bruno, Pascal Forrer, Frank Kolbinger, Stephen Oliver, Peter Gergely, Tobias Junt, and Isabelle Isnardi for useful discussions. We are grateful to Jonas Zierer and Lucia Csepregi for their helpful comments. We thank the following principal investigators in the hidradenitis suppurativa study (NCT02421171): Gregor Jemec, Christos C. Zouboulis, Falk G. Bechara, Matthew Zook, Lars French, Robert Hunger, Barbara Hováth, Sylke Schneider-Burns, James A. Solomon, Michael H. Gold, Howard Sofen, Joel Schlessinger, Benjamin N. Lockshin, Kenneth W. Dawes, Jan Mekkes, and Christian Vestergaard. We also thank Izabela Rozenberg, Philip Jarvis, and Thomas Peters for their respective roles in hidradenitis suppurativa study (NCT02421171). This work was supported by Novartis Institutes for BioMedical Research.

AUTHOR CONTRIBUTIONS

Conceptualization: AA, BR, CL, ET, TAR, VC; Formal Analysis: AA, AS, BR, ET, GM, GW, JCUL, LR, SG, VC, YW; Investigation: AA, AH, AS, AW, BR, CC, EPP, ET, GM, GW, HT, JCUL, JFG, JR, LR, MC, TAR, UN, VC, YW; Methodology: AA, AS, AW, BR, CC, ET, GM, GW, HT, JCUL, JEG, JFG, JR, LR, MC, UN, YW; Resources: BWL, DJS, EFF, EPP, JEG, PM, RDR, RO, SKG, SOC; Supervision: AA, AS, BR, EPP, ET, GW, JCUL, LR, TAR; Writing − Original Draft Preparation: BR, GM, TAR; Writing − Review and Editing: AA, BR, EFF, EPP, ET, GM, JEG, LR, TAR, VC

SUPPLEMENTARY MATERIAL

Supplementary material is linked to the online version of the paper at www.jidonline.org, and at https://doi.org/10.1016/j.jid.2022.08.051

REFERENCES

Baumann T, Dunkel A, Schmid C, Schmitt S, Hiltensperger M, Lohr K, et al. Regulatory myeloid cells paralyze T cells through cell-cell transfer of the metabolite methylglyoxal. Nat Immunol 2020;21:555−66.

Byrd AS, Carmona-Rivera C, O'Neil LJ, Carlucci PM, Cisar C, Rosenberg AZ, et al. Neutrophil extracellular traps, B cells, and type I interferons contribute to immune dysregulation in hidradenitis suppurativa. Sci Transl Med 2019;11:eaav5908.

Carlavan I, Bertino B, Rivier M, Martel P, Bourdes V, Motte M, et al. Atrophic scar formation in patients with acne involves long-acting immune responses with plasma cells and alteration of sebaceous glands. Br J Dermatol 2018;179:906−17.

Carmona-Rivera C, O'Neil LJ, Patino-Martinez E, Shipman WD, Zhu C, Li QZ, et al. Autoantibodies present in hidradenitis suppurativa correlate with disease severity and promote the release of proinflammatory cytokines in macrophages. J Invest Dermatol 2022;142:924−35.

Chen WT, Chi CC. Association of hidradenitis suppurativa with inflammatory bowel disease: A systematic review and meta-analysis. JAMA Dermatol 2019;155:1022−7.

Collins AM, Jackson KJ. A temporal model of human IgE and IgG antibody function. Front Immunol 2013;4:235.

Constantinou CA, Fragoulis GE, Nikiphorou E. Hidradenitis suppurativa: infection, autoimmunity, or both? Ther Adv Musculoskelet Dis 2019;11:1759720X19895488.

Corbière V, Segers J, Desmet R, Lecher S, Loyens M, Petit E, et al. Natural T cell epitope containing methyl lysines on mycobacterial heparin-binding hemagglutinin. J Immunol 2020;204:1715−23.

Czarnowicki T, Gonzalez J, Bonifacio KM, Shemer A, Xiangyu P, Kunjravia N, et al. Diverse activation and differentiation of multiple B-cell subsets in patients with atopic dermatitis but not in patients with psoriasis. J Allergy Clin Immunol 2016;137:118−29.e5.

Defendenti C, Grosso S, Atzeni F, Croce A, Senesi O, Saibeni S, et al. Unusual B cell morphology in inflammatory bowel disease. Pathol Res Pract 2012;208:387−91.

Der Sarkissian S, Hessam S, Kirby JS, Lowes MA, Mintoff D, Naik HB, et al. Identification of biomarkers and critical evaluation of biomarkers validation in hidradenitis suppurativa: a systematic review [published correction appears in JAM Dermatol 2022;158:590]. JAMA Dermatol 2022;158:300−13.

Figueras-Nart I, Mascaró JM Jr, Solanich X, Hernández-Rodríguez J. Dermatologic and dermatopathologic features of monogenic autoinflammatory diseases. Front Immunol 2019;10:2448.

Fletcher JM, Moran B, Petrasca A, Smith CM. IL-17 in inflammatory skin diseases psoriasis and hidradenitis suppurativa. Clin Exp Immunol 2020;201:121−34.

Galligan JJ, Wepy JA, Streeter MD, Kingsley PJ, Mitchener MM, Wauchope OR, et al. Methylglyoxal-derived posttranslational arginine modifications are abundant histone marks. Proc Natl Acad Sci USA 2018;115:9228−33.

Gudjonsson JE, Tsoi LC, Ma F, Billi AC, van Straalen KR, Vossen ARJV, et al. Contribution of plasma cells and B cells to hidradenitis suppurativa pathogenesis. JCI Insight 2020;5.

Guedj K, Abitbol Y, Cazals-Hatem D, Morvan M, Maggiori L, Panis Y, et al. Adipocytes orchestrate the formation of tertiary lymphoid organs in the creeping fat of Crohn's disease affected mesentery. J Autoimmun 2019;103:102281.

Halliley JL, Tipton CM, Liesveld J, Rosenberg AF, Darce J, Gregoretti IV, et al. Long-lived plasma cells are contained within the CD19(-)CD38(hi)CD138(+) subset in human bone marrow. Immunity 2015;43:132−45.

Hua VJ, Kilgour JM, Cho HG, Li S, Sarin KY. Characterization of comorbidity heterogeneity among 13,667 patients with hidradenitis suppurativa. JCI Insight 2021;6:e151872.

Kitani A, Strober W. Regulation of C gamma subclass germ-line transcripts in human peripheral blood B cells. J Immunol 1993;151:3478−88.

Kromann CB, Deckers IE, Esmann S, Boer J, Prens EP, Jemec GB. Risk factors, clinical course and long-term prognosis in hidradenitis suppurativa: a cross-sectional study. Br J Dermatol 2014;171:819−24.

Lobo PI. Role of natural autoantibodies and natural IgM anti-leucocyte autoantibodies in health and disease. Front Immunol 2016;7:198.

Maessen DE, Stehouwer CD, Schalkwijk CG. The role of methylglyoxal and the glyoxalase system in diabetes and other age-related diseases. Clin Sci (Lond) 2015;128:839−61.

Mulani S, McNish S, Jones D, Shanmugam VK. Prevalence of antinuclear antibodies in hidradenitis suppurativa. Int J Rheum Dis 2018;21:1018−22.

Musilova J, Moran B, Sweeney CM, Malara A, Zaborowski A, Hughes R, et al. Enrichment of plasma cells in the peripheral blood and skin of patients with hidradenitis suppurativa. J Invest Dermatol 2020;140:1091−4.e2.

Penno CA, Jäger P, Laguerre C, Hasler F, Hofmann A, Gass SK, et al. Lipidomics profiling of hidradenitis suppurativa skin lesions reveals lipoxygenase pathway dysregulation and accumulation of proinflammatory leukotriene B4. J Invest Dermatol 2020;140:2421−32. e10.

Pisetsky DS. Antinuclear antibodies in rheumatic disease: a proposal for a function-based classification. Scand J Immunol 2012;76:223−8.

Prens E, Deckers I. Pathophysiology of hidradenitis suppurativa: an update. J Am Acad Dermatol 2015;73:S8−11.

Principi M, Cassano N, Contaldo A, Iannone A, Losurdo G, Barone M, et al. Hydradenitis suppurativa and inflammatory bowel disease: an unusual, but existing association. World J Gastroenterol 2016;22:4802−11.

Richette P, Molto A, Viguier M, Dawidowicz K, Hayem G, Nassif A, et al. Hidradenitis suppurativa associated with spondyloarthritis – results from a multicenter national prospective study. J Rheumatol 2014;41:490−4.

Savage KT, Flood KS, Porter ML, Kimball AB. TNF-α inhibitors in the treatment of hidradenitis suppurativa. Ther Adv Chronic Dis 2019;10:2040622319851640.

Schalkwijk CG, Stehouwer CDA. Methylglyoxal, a highly reactive dicarbonyl compound, in diabetes, its vascular complications, and other age-related diseases. Physiol Rev 2020;100:407−61.

Shamsaldeen YA, Mackenzie LS, Lione LA, Benham CD. Methylglyoxal, A metabolite increased in diabetes is associated with insulin resistance,

vascular dysfunction and neuropathies. Curr Drug Metab 2016;17:359–67.

Shibayama R, Araki N, Nagai R, Horiuchi S. Autoantibody against N(epsilon)-(carboxymethyl)lysine: an advanced glycation end product of the Maillard reaction. Diabetes 1999;48:1842–9.

Søreide K. Receiver-operating characteristic curve analysis in diagnostic, prognostic and predictive biomarker research. J Clin Pathol 2009;62:1–5.

Soto-Heredero G, Gómez de Las Heras MM, Gabandé-Rodríguez E, Oller J, Mittelbrunn M. Glycolysis - a key player in the inflammatory response. FEBS Journal 2020;287:3350–69.

Spergel JM, Paller AS. Atopic dermatitis and the atopic march. J Allergy Clin Immunol 2003;112:S118–27.

Turk Z, Ljubic S, Turk N, Benko B. Detection of autoantibodies against advanced glycation endproducts and AGE-immune complexes in serum of patients with diabetes mellitus. Clin Chim Acta 2001;303:105–15.

Tzanetakou V, Kanni T, Giatrakou S, Katoulis A, Papadavid E, Netea MG, et al. Safety and efficacy of anakinra in severe hidradenitis suppurativa: a randomized clinical trial [published correction appears in JAM Dermatol 2017;153:950]. JAMA Dermatol 2016;152:52–9.

van der Zee HH, de Ruiter L, Boer J, van den Broecke DG, den Hollander JC, Laman JD, et al. Alterations in leucocyte subsets and histomorphology in normal-appearing perilesional skin and early and chronic hidradenitis suppurativa lesions. Br J Dermatol 2012;166:98–106.

Vanlaerhoven AMJD, Ardon CB, van Straalen KR, Vossen ARJV, Prens EP, van der Zee HH. Hurley III hidradenitis suppurativa has an aggressive disease course. Dermatology 2018;234:232–3.

Vidarsson G, Dekkers G, Rispens T. IgG subclasses and allotypes: from structure to effector functions. Front Immunol 2014;5:520.

Vistoli G, De Maddis D, Cipak A, Zarkovic N, Carini M, Aldini G. Advanced glycoxidation and lipoxidation end products (AGEs and ALEs): an overview of their mechanisms of formation. Free Radic Res 2013;47(Suppl. 1):3–27.

von der Werth JM, Williams HC. The natural history of hidradenitis suppurativa. J Eur Acad Dermatol Venereol 2000;14:389–92.

Wang C, Turunen SP, Kummu O, Veneskoski M, Lehtimäki J, Nissinen AE, et al. Natural antibodies of newborns recognize oxidative stress-related malondialdehyde acetaldehyde adducts on apoptotic cells and atherosclerotic plaques. Int Immunol 2013;25:575–87.

SUPPLEMENTARY MATERIALS AND METHODS

Serum samples from patients with hidradenitis suppurativa

The sera of patients in cohort 1 were taken from patients with hidradenitis suppurativa (HS) during their baseline visit as part of a proof-of-concept, phase 2 randomized clinical trial of CJM112, a human anti−IL-17A/IL-17AF high-affinity IgG1κ mAb in HS (NCT02421171). Briefly, all patients were adults aged between 18 and 65 years with chronic moderate-to-severe HS for at least 1 year before screening and who had previously undergone antibiotic therapy. Moderate-to-severe HS was defined as having an HS Physician's Global Assessment score of at least moderate severity (score $\geq$ 3) and with at least four abscesses and/or nodules. Additional inclusion criteria required patients to have HS lesions in at least two anatomical areas, and at least one area had to be minimally Hurley stage 2. Patients receiving systemic treatment (including retinoids and immunomodulatory therapies) or antibiotics were required to stop treatment at least 4 weeks before randomization. Patients previously treated with IL-17 pathway inhibitors, including secukinumab, ixekizumab, and brodalumab, were excluded from the study. Adequate wash-out periods were applied for patients treated with biologics; no wash-out period was requested for treatment with topicals. A further list of inclusion and exclusion criteria can be found at clinicaltrials.gov (Identifier: NCT02421172). Only baseline samples (i.e., untreated at the time of collection) from patients who signed written informed consent for exploratory biomarker analysis were used. Patient characteristics collected as part of the study are summarized in Supplementary Table S2.

Serum samples from patients without HS

The sera of patients with acne were taken from patients during their baseline visit as part of a proof-of-concept, phase 2 randomized clinical trial of CJM112 in acne vulgaris (NCT02998671). Only baseline samples (i.e., untreated at the time of collection) from patients who signed written informed consent for exploratory biomarker analysis were used.

Serum samples from patients with atopic dermatitis, ulcerative colitis, and Crohn's disease were purchased from BioIVT (Westbury, NY). As per recruiting proceeding, all patients donating human material to BioIVT signed an informed consent accepting the use of such material for exploratory research.

Plasma samples from patients with HS

The plasma from patients in cohort 2 was collected from 40 patients with HS recruited through the HS outpatient clinic of the Department of Dermatology, Erasmus University Medical Center (Rotterdam, The Netherlands). Briefly, all patients were adults aged between 18 and 62 years with a clinical diagnosis of HS for at least 1 year before sample collection. No exclusions were made regarding severity or previous or ongoing treatment. All samples were obtained with written informed consent from the participants in accordance with the Declaration of Helsinki principles. The study protocol was approved by the Institutional Review Board of the Erasmus University Medical Center (MEC-2016-426). The patient characteristics are listed in Supplementary Table S2.

Serum and plasma samples from healthy volunteers

Healthy volunteer (HV) serum controls (n = 22; aged 28−70 years, mean = 50 years, median = 52 years; three males [14%], 19 females [86%]), used in Figure 1 and Supplementary Figure S1, were purchased from BioIVT. As per recruiting proceeding, all patients donating human material to BioIVT signed an informed consent accepting the use of such material for exploratory research.

Plasma from HVs (n = 34; aged 25−80 years, mean = 36−46 years, median = 37−47 years; 19 males [56%], 15 females [44%]), as used in Figure 3 and Supplementary Figures S2 and S6, was obtained under written informed consent either through the Novartis Tissue Donor Program (TRI0128; 2017-00271) or from the University Hospital Basel (Basel, Switzerland), as part of noninterventional biomarker study BASICHR0043 (2019-02188). Both are in accordance with the Swiss Human Research Act and approval of the responsible ethics committee (Ethikkommission Nordwest- und Zentralschweiz number: 329/13).

Specific details of healthy control samples are listed in Supplementary Table S4. Note that to ensure confidentiality, the ages of Novartis Tissue Donor Program donors are only provided as range data.

HS skin samples from Basel and Baselland, Switzerland

Skin from patients with HS undergoing surgical excision was received from the Department of Plastic, Reconstructive, Aesthetic and Hand Surgery of University Hospital Basel (Basel, Switzerland); from the Clinic for General, Visceral, Vascular and Thoracic surgery, Cantonal Hospital Baselland (Liestal, Switzerland); or from Praxis beim Merian Iselin (Basel, Switzerland) as part of noninterventional biomarker studies TRI1270397 and BASICHR0043. All patients provided written informed consent, and the study was conducted in accordance with the ethical principles originating in the Declaration of Helsinki and was approved by the local Ethics Committee (EKNZ 2016-01204; EKNZ 2019-02188). The anatomical sites of excisions were inconsistently recorded and are not tracked in this manuscript.

HS skin samples from Rotterdam, Netherlands

Patients with moderate-to-severe HS undergoing surgery were recruited from the HS outpatient clinic of the Department of Dermatology, Erasmus University Medical Center. Patients had ceased any previous topical or systemic treatment at least 2 weeks before enrollment. Biopsies from lesional skin were collected from resected tissue after routine surgery. Lesional tissue was defined on the basis of the presence of nodules/abscesses and/or tunnels. Lesional tissue was not differentially segregated on the basis of the presence or absence of tunnels. The study protocol was approved by the Institutional Review Board of the Erasmus University Medical Center (MEC-2013-337) and was conducted in accordance with the ethical principles originating in the Declaration of Helsinki. The anatomical sites of excisions were inconsistently recorded and are not tracked in this manuscript.

Autoantigens

All autoantigens screened in this study were obtained from commercial sources, except for flagellin, which was

conjugated to BSA internally (see the paragraph below). The list of autoantigens, the commercial vendors, and catalog numbers as well as the rationale for their inclusion are summarized in Supplementary Table S1.

BSA-conjugated flagellin modification

Flagellin (catalog number TLRL-BSFLA, Invivogen, San Diego, CA) was reconstituted by reverse pipetting with LAL water (catalog number H2OLAL-1.5, Invivogen) to obtain a solution at 1 mg/ml. A 1 g of BSA (catalog number 001-000-162, Jackson ImmunoResearch, West Grove, PA) was dissolved in 50 ml of demineralized water to obtain a stock solution at 20 mg/ml. A total of 100 mg of N-(3-Dimethylaminopropyl)-N′-ethylcarbodiimide hydrochloride (catalog number E1769-5g, Sigma-Aldrich, St. Louis, MO) were dissolved in 2 ml of demineralized water to obtain a stock solution at 50 mg/ml. A total of 50 μl of flagellin at 1 mg/ml were mixed in a micronic tube (32022-MIC, Vitaris, Baar, Switzerland) with 2.5 μl of BSA at 20 mg/ml and 10 μl of N-(3-Dimethylaminopropyl)-N′-ethylcarbodiimide hydrochloride at 50 mg/ml. The solution was incubated overnight at +4 °C with slow agitation on a rotor to allow the coupling of flagellin on BSA. The purification of BSA-conjugated flagellin was performed through dialysis. Dialysis units (Slide-A-Lyser Mini Dialysis Units [10,000 MWCO, 0.1 ml]) (catalog number 69570, Thermo Fisher Scientific, Waltham, MA) with the buoys (catalog number 69588, Thermo Fisher Scientific) were put for 10 minutes into 2 l of dialysis buffer (PBS) (catalog number 14733200, Roche, Basel, Switzerland). The solution containing BSA-conjugated flagellin was added to the dialysis unit and dialyzed for 1 hour at room temperature. The dialysis buffer was changed every hour three times. The purified solution of BSA-conjugated flagellin, with a final concentration of 800 μg/ml, was then stored at −20 °C.

Autoantibody profiling

Autoantibodies were detected using a custom-made Luminex assay on the basis of magnetic beads. All washing steps of magnetic beads in tubes and plates were performed with the support of magnetic separation plates. Briefly, 100 μl of stock solution of Luminex magnetic beads were prewashed twice with 200 μl of Tris-buffered saline (TBS) (T9039, Sigma-Aldrich) in micronic tubes (Vitaris, 32022-MIC) and then resuspended in 200 μl of coating solution containing antigens at 20 μg/ml in TBS. After overnight incubation at +4 °C with continuous rolling and cover from light, beads were washed twice with 200 μl of 0.05% TBS-Tween (T9039, Sigma-Aldrich) and then blocked with 400 μl of blocking solution for 2 hours at room temperature, with continuous rolling and cover from light. The blocking solution was composed of TBS with non-fat milk (T8793, Sigma-Aldrich) at 3%, fetal bovine serum (FBS) (10082-147, Gibco, Waltham, CA) at 10%, and Proclin300 (48912U, Sigma-Aldrich) at 0.1%. Before plate loading, Luminex beads were mixed and washed once with 1 ml of 0.05% TBS-Tween and Proclin300 at 0.1% and then resuspended with 10.4 ml of 0.05% TBS-Tween and Proclin300 at 0.1%. Before being loaded on plates, serum or plasma samples were diluted at 1:100 in 0.05% TBS Tween, 10% FBS, 1% non-fat milk, and 0.1% BSA (001-000-162, Jackson ImmunoResearch). A total of 100 μl/well of diluted serum were loaded on a black polystyrene plate (3915, Costar, Corning, New York, NY) together with 25 μl/well of prepared magnetic beads. After 1 hour of incubation at room temperature with stirring at 750 r.p.m. and cover from light, the plate was washed twice with 300 μl/well of 0.05% TBS-Tween using an automatic washer (Elx405UM, Biotek, Winooski, VT) combined with a magnetic separation plate and 3 minutes of waiting time before and after the first wash. After washing, 100 μl/well of phycoerythrin-tagged detection antibody targeting IgG, IgG1, IgG2, IgG3, IgG4, IgM, or IgA (2040-09, 9054-09, 9070-09, 9210-09, 9190-09, 2020-09, 2050-09, Southern Biotech, Birmingham, AL), respectively, at 0.5 μg/ml and 1 μg/ml for IgG subclasses and 0.2 μg/ml and 1 μg/ml in 0.05% TBS-Tween were added and incubated on plate for 1 hour at room temperature with stirring at 750 r.p.m. and cover from light. The plate was then washed twice with 300 μl/well of 0.05% TBS-Tween using an automatic washer coupled with a magnetic separation plate and 3 minutes of waiting time before and after the first wash. A total of 120 μl/well of TBS, 0.5% BSA, and 0.1% Proclin300 were then added to the plate. After 3 minutes of incubation at room temperature with a stirring of 750 r.p.m. and cover from light to resuspend the beads, the plate was read using the Flexmap3D reader. Results were reported using the median fluorescence index as the unit of measure.

Incubation with carboxyethyl lysine, carboxy-methyl-lysine, and octopine before autoantibodies profiling assay

To test the specificity of anti-carboxyethyl lysine (CEL) autoantibodies, plasma samples were diluted at 1:100 with dilution buffer (0.05% TBS-Tween, 10% FBS, 1% non-fat milk, 0.1% BSA, 0.1% Proclin300) containing 50 μg/ml of either CEL (25333, Cayman Chemical, Ann Arbor, MI), carboxy-methyl-lysine (16483, Cayman Chemical), or octopine (MBS6045660, MyBiosource, San Diego, CA). The samples were incubated for 30 minutes at room temperature before proceeding with the autoantibodies assay. Control samples diluted with a buffer not containing CEL, carboxy-methyl-lysine, or octopine were also incubated for 30 minutes at room temperature before proceeding with the autoantibodies assay.

Methylglyoxal modification of histone

Methylglyoxal-modified histone was prepared using a protocol described by Srey et al. (2010). Recombinant human histone H2A was dialyzed against PBS before the Methylglyoxal-modification reaction. Specifically, histone H2A (H2042, Sigma-Aldrich) at 0.1 mg/ml was mixed with sodium pyruvate (S8636, Sigma-Aldrich) (17.14 mM) and sodium cyanoborohydride (156159, Sigma-Aldrich) (25.71 mM) in PBS (11666789001, Sigma-Aldrich) (0.1 M, pH 7.0). The solution was incubated at 37 °C for 24 hours and then abundantly dialyzed against PBS. A control was also prepared using the same conditions but with the omission of sodium pyruvate.

CEL detection by direct ELISA

A total of 2-mm punch biopsies of lesional HS skin were immersed in liquid nitrogen using Covaris tissue tubes TT05 (520071, Covaris, Woburn, MA) and crushed with a CP02 cryoPREP Automated Dry Pulverizer (500001, Covaris). The fragments of skin were collected and weighted and then resuspended with 50 µl of 0.05% TBS-Tween Triton 1% X-100 (T8787, Sigma-Aldrich). These solutions were then sonicated five times for 30 seconds and vortexed between each sonication. Skin lysates were then diluted at 1:10 in PBS (11666789001, Sigma-Aldrich). A total of 50 µl/well of diluted skin lysates and standards (CEL BSA from Cell Biolabs, San Diego, CA, STA-302, at different concentrations in PBS) were loaded on an ELISA plate and incubated overnight at 4 °C with stirring at 400 r.p.m. and cover from light. The plate was then washed four times with 300 µl/well of 0.05% PBS Tween (P3563, Sigma-Aldrich) and blotted against a tissue. The plate was blocked with 150 µl/well of 3% PBS BSA (BSA from Roche, 10735078001) for 1 hour at room temperature, with stirring at 500 r.p.m. and cover from light. The plate was then washed four times with 300 µl/well of 0.05% PBS Tween and blotted against a tissue. A total of 100 µl/well of biotinylated anti-CEL mAb (clone KNH30, MAB6594, Abnova, Taipei, Taiwan) diluted at 1:250 in 0.05% PBS Tween were loaded on the plate and incubated for 2 hours at room temperature, with stirring at 500 r.p.m. and cover from light. The plate was then washed four times with 300 µl/well of 0.05% PBS Tween and blotted against a tissue. A total of 100 µl/well of Streptavidin-horseradish peroxidase (DY998, R&D System, Minneapolis, MN) diluted at 1:200 were loaded on the plate and incubated for 30 minutes at room temperature, with stirring at 500 r.p.m. and cover from light. The plate was then washed four times with 300 µl/well of 0.05% PBS Tween and blotted against a tissue. A total of 100 µl/well of Ultra TMB (34028, Thermo Fisher Scientific) were loaded on the plate and incubated for 1 hour at room temperature. Finally, 100 µl/well of Sulfuric acid (38291, Fluka, Buchs, Switzerland) at 1 M was added, and plate optic deviance was read at 450 nm.

Linear combination of disease severity and disease duration

We used a refined Hurley score to define disease severity, and we transformed the seven categories (1a, 1b, 1c, 2a, 2b, 2c, and 3) into numerical values from 1 to 7. Disease duration was expressed in years and calculated as follows:

$$\text{Disease duration} = \text{Patient's age} - \text{age at disease onset}$$

Both numerical disease severity and disease duration for each patient were then standardized by dividing by the average, as follows:

$$\text{Std disease severity (patient n)} = \frac{\text{disease severity (patient n)}}{\text{disease severity average}}$$

$$\textit{Std}\text{ disease duration (patient n)} = \frac{\text{disease duration (patient n)}}{\text{disease duration average}}$$

Standardized values were then combined by Euclidean distance, which was calculated using Pythagoras:

$$\text{Combination} = \sqrt{(\text{Std severity})^2 + (\text{Std duration})^2}$$

The overall formula used to calculate the linear combination of disease severity and duration is then as follows:

$$\text{Combination (patient n)} = \sqrt{\left(\frac{\text{disease severity (patient n)}}{\text{disease severity average}}\right)^2 + \left(\frac{\text{disease duration (patient n)}}{\text{disease duration average}}\right)^2}$$

See also Supplementary Figure S2b–e for a graphical depiction of this calculation.

HS skin digestion

Overnight digestion protocol (Basel, Switzerland). Fresh HS skin discards were processed within 3 hours after surgery. After removal of the fat layer, the skin was cut into small pieces, washed multiple times with wash buffer (RPMI1640 Glutamax medium, 25 mM 4-[2-hydroxyethyl]-1-piperazineethanesulfonic acid, 100 U/100 µg penicillin/streptomycin, 50 µg/ml gentamicin), and digested overnight with wash buffer supplemented with 100 µg/ml collagenase P (Roche), 3 µM calcium chloride (Fluka), and 10% fetal calf serum (PAALaboratories, Cölbe, Germany). After digestion, 1 mg/ml DNAse1 (Sigma-Aldrich) was added and incubated for a further 30 minutes at 37 °C. The digested cell suspension was filtered through cell strainers (Corning, Corning, NY), and erythrocytes were lysed by incubating the suspension in erythrocyte lysis buffer Buffer EL (number 79217, Qiagen, Hilden, Germany) at room temperature for 5 minutes. Cells were then washed and counted using a Countess II Automated Cell Counter (Life Technologies, Carlsbad, CA), and the single-cell suspension was then frozen in 10% DMSO and 90% fetal calf serum at 50–100 × 10^6 cells/vial aliquots

and stored for 1−2 days at −80 °C before transfer into liquid nitrogen.

Short digestion protocol (Rotterdam, Netherlands). Samples were sourced from surgically excised lesional skin derived from patients with severe HS. Prepared on ice, samples were extensively minced using surgical scissors and subsequently incubated for 1.5 hours in 50 μG/ml (328.3 U/ml) LiberaseTM (Roche) in RPMI1640 (Lonza, BioWhittaker, Walkersville, MD) at 37 °C, followed by a 10-minute incubation in 100 μG/ml DNase I (Roche). Samples were then washed with 5% FBS (Life Technologies) in RPMI and strained through a 70-μM mesh (Corning). The resultant single-cell suspension was then frozen down in 10% DMSO (Merck, Kenilworth, NJ) and 90% FBS (Life Technologies).

Flow cytometry sorting experiments

Cells were thawed at 37 °C and washed in PBS. Cell suspensions were resuspended in PBS containing LIVE/DEAD Fixable Aqua Dead Cell Stain (L34957, Thermo Fisher Scientific) for 15 minutes according to the manufacturer's instructions for the exclusion of dead cells. Cell suspensions were then washed twice in phenol red−free tissue culture media (RPMI 1640 Medium, no phenol red [Gibco by Life Technologies], 10% fetal calf serum [GE Healthcare, Chicago, IL], penicillin−streptomycin 10,000 U/ml [Gibco by Life Technologies]) before the cells were resuspended in phenol red−free tissue culture media containing antibody cocktail for 1 hour at 4 °C. Cells were then washed twice more in phenol red−free tissue culture media and filtered through 70-μm cell strainers (Corning). Cells were sorted using a FACSCanto II (BD Biosciences, San Jose, CA) (see Supplementary Figure S5a). Purity checks were routinely run after sorting to assess the fidelity of the sort.

Flow cytometry acquisition experiments

Cells were thawed at 37 °C and washed in running buffer (PBS [Gibco], 1% fetal calf serum [GE Healthcare], EDTA [Gibco], and 0.05% sodium azide [Sigma-Aldrich]). Cell suspensions were resuspended and antibody stained in running buffer for 1 hour at 4 °C. Cells were washed, filtered, and analyzed on either a 5-laser LSRFortessa (BD Biosciences) or a 5-laser. Cytek Aurora spectral flow cytometer using SpectroFlo software (Cytek Biosciences, Fremont, CA). Flow cytometry data were analyzed using FlowJo software (version 10.6.0, BD Biosciences).

Flow cytometry antibodies

The antibodies used in this study for flow cytometry (acquisition and sorting) were CD3 allophycocyanin (APC) (clone SK7, Thermo Fischer Scientific), CD3 BUV737 (clone SK7, BD Biosciences), CD19 BV711 (clone SJ25-C1, BD Biosciences), CD19 BV785 (clone HIB19, BioLegend, San Diego, CA), CD20 BV421 (clone 2H7, BD Biosciences), CD20 BV421 (clone Clone 2H7, BD Biosciences), CD20 BV650 (clone 2H7, BioLegend), CD27 V450 (clone M-T271, BD Biosciences), CD38 APC-Cy7 (clone HIT2, BioLegend), CD38 PE-Cy7 (clone HIT2, BD Biosciences), CD38 PE-Cy7 (clone HIT2, BioLegend), CD45 APC-Cy7 (clone 2D1, BD Biosciences), CD45 BUV395 (clone HI30; BD Biosciences), CD86 BUV737 (clone 2331 [FUN-1], BD Biosciences), CD63 Alexa Fluor 647 (clone H5C6, BD Biosciences), CD138 APC (clone MI15, BioLegend), HLA-DR PerCP-Cy5.5 (clone L243, BioLegend), IgA FITC (polyclonal antibody, Jackson ImmunoResearch), IgA1 APC (clone SAA1, Cytogenos, Salamanca, Spain), IgA1 PerCP/Cy5.5 (clone SAA1, Cytogenos), IgA2 PerCP/Cy5.5 (clone SAA2, Cytogenos), IgD APC/Cy7 (clone IA6-2, BioLegend), IgD PE (clone IA6-2, BD Biosciences), IgD PE-Cy7 (clone IA6-2, BioLegend), IgG Alexa Fluor 647 (polyclonal antibody, Jackson ImmunoResearch), IgG1 PE (clone SAG1, Cytogenos), IgG2 FITC (clone SAG2, Cytogenos), IgG2 PE (clone SAG2, Cytogenos), IgG3 FITC (clone SAG3, Cytogenos), IgG4 APC (clone SAG4, Cytogenos), and IgM PE (polyclonal antibody, Jackson ImmunoResearch).

Antigen-specific and total Ig detection by enzyme-linked immunosorbent spot

For antigen-specific and total Ig-secreting cell detection, 96-well enzyme-linked immunosorbent spot plates (Millipore MSIPS4510 Sterile, hydrophobic high protein binding immobilon-P membrane) were coated with 1 μg/ml purified unlabeled goat anti-human IgG or IgA or IgM (2040-01, 2050-01, and 2020-01, respectively, Southern Biotech) or 5 μg/ml CEL antigen (25333, Cayman Chemical) for 2 hours at room temperature. After washing with PBS solution, the plates were blocked with 1% BSA in PBS and incubated for 30 minutes at 37 °C. B cells and plasmablasts sorted from HS skin were added in a final volume of 200 μl of basic medium prepared using RPMI 1640 (number 11875-093, Gibco) supplemented with 10% fetal bovine serum (number SH3007.03, HyClone, Thermo Fisher Scientific), 1 mM sodium pyruvate (number 11360-070, Gibco), MEM nonessential amino acids (100 μM each, number 11140-050, Gibco), 50 μM b-mercaptoethanol (number 31350-010, Gibco), penicillin/streptomycin (number P4333, Sigma-Aldrich), and kanamycin (100 μg/ml, Gibco, Life Technologies) and incubated overnight at 37 °C. Next, the plates were washed three times with 0.25% PBS Tween 20 and four times with PBS and incubated for 2 hours at room temperature with Ig-specific, biotin-conjugated secondary antibody (2043-08, 2050-08, 2020-08, Southern Biotech). After washing, avidin-peroxidase (A3151, Sigma-Aldrich) was added and left for 1 hour at room temperature. The assay was developed with AEC (A6926, Sigma-Aldrich). For quantification of antibody-secreting cells, plates were acquired, counted, and quality controlled using an enzyme-linked immunosorbent spotreader and ImmunoSpot 5.1 software (CTL Europe, Bonn, Germany).

Complement activation assay

For the complement activation experiments (Supplementary Figure S6), a 96-well high binding plate (655061, Greiner Bio-One, Monroe, NC) was first coated overnight at 4 °C with 10 μg/ml CEL BSA (STA-302, Cell Biolabs). The plate was then washed three times with PBS with 0.05% Tween 20 (524653-1EA, Calbiochem, San Diego, CA) and blocked with blocking buffer (37539, Thermo Fisher Scientific) for 1 hour at room temperature, followed by washing three times with PBS with 0.05% Tween 20. Plasma from patients with HS or HVs was diluted at 1:10 in PBS before loading on the plate. After 30 minutes of incubation at room temperature, the plate was washed twice with PBS Tween and once with PBS (10010-015, Gibco). The complement-preserved serum pool

of healthy donors was collected through the Basel Tissue Donor Program in accordance with the ethical principles originating in the Declaration of Helsinki, and was added to the plate and incubated for 1 hour at 37 °C. As an indication of the complement activation, the level of terminal complement complex sC5b-9 in each sample was quantified with ELISA (A020, QuidelOrtho, San Diego, CA) according to the manufacturer's instructions.

Single-cell RNA-sequencing data

The single-cell RNA-sequencing data from lesional HS skin was previously described (Gudjonsson et al., 2020). The candidate plasma cell markers were obtained by contrasting the plasma cells to the B cells with the findMarkers function from the scran (Lun et al., 2016) R package (1.18.5). The test type was set to *t*-test, and the blocking level was set to the donor identifications. The resultant volcano plot (Supplementary Figure S4a) was created using GraphPad Prism, version 9 (GraphPad Software, La Jolla, CA). The dot plots of cell clusters displaying the average gene expression and frequency of positive cells (Supplementary Figure S4b) were generated using R package ggplot2 (Wickham, 2016). All R calculations were run with R-4.0.3.

Affymetrix data

The generation of the RNA expression data from healthy, lesional HS, and nonlesional HS skin (Figure 4i) has previously been described (Penno et al., 2020) (dataset available through the Gene Expression Omnibus, GSE148027). Data shown in Figure 4i are robust multichip average–normalized expression values of Affymetrix data. The heatmap shown in Figure 4i was created using GraphPad Prism, version 9.

Conventional histology

To assess HS pathology, large (1–2 cm^2) tissue fragments were cut from resected HS skin and fixed in 10% v/v neutral phosphate-buffered formalin solution (J.T. Baker, catalog number 3933.9010, Avantor, Radnor Township, PA) for 24 hours at room temperature and then transferred to 50% ethanol and 50% dihydrogen oxide and stored at 4 °C until processing. Fixed skin samples were dehydrated through a graded series of ethanol concentrations (50–100%), cleared with xylene, and infiltrated with paraffin overnight using the vacuum infiltration tissue processor (Leica ASP200S, Leica Biosystems, Muttenz, Switzerland). On the following day, the tissue was embedded in paraffin blocks. HS tissue was sectioned (3 μm) and stained with H&E by MC or CC at Autoimmunity, Transplantation and Inflammation (ATI) Disease Area, Novartis Institutes for BioMedical Research, Novartis Pharma AG (Basel, Switzerland). Samples were imaged using a ScanScope XT slide scanner (Aperio, Leica Biosystems) at ×40 magnification.

Chromogenic immunohistochemistry

Automated immunohistochemical stainings for CD20 and CD21 were performed using a Ventana Discovery XT automated stainer (Roche) by MC or CC at Autoimmunity, Transplantation and Inflammation (ATI) Disease Area, Novartis Institutes for BioMedical Research, Novartis Pharma AG. Specific isotype controls were used as negative controls. Samples were digitalized using an Aperio ScanScope XT slide scanner (Leica Biosystems). Exemplary images in JPEG format were taken using the Aperio ImageScope software, version 12.3.2.8013 (Leica Biosystems).

Spatial transcriptomics

Fluorescent labeling and spatial transcriptomics (Merritt et al., 2020) were performed by NanoString Technologies through the Technology Access Program (NanoString Technologies, Seattle, WA). Specifically, formalin-fixed, paraffin-embedded blocks from discarded tissue of patients with HS were preselected and sectioned, and adjacent control sections were costained for CD20 (see histology methods) at Autoimmunity, Transplantation and Inflammation (ATI) Disease Area, Novartis Institutes for BioMedical Research, Novartis Pharma AG for spatial transcriptomic profiling using the HuWTA (Human Whole Transcriptome Atlas). Sections were processed according to NanoString GeoMx DSP (Digital Spatial Profiling) guidelines. Briefly, after deparaffinization and antigen retrieval procedures, sections were incubated with Whole Transcriptome Atlas probes overnight at 37 °C. On the next day, the slides were washed and stained with fluorescently labeled antibodies against pan-cytokeratin (Alexa Fluor 647, clone AE1+AE3, number NBP2-33200AF647, Novus Biologicals, Littleton, CO), CD20 (Alexa Fluor 594, clone IGEL/773, number NBP2-47840DL594, Novus Biologicals), and Vimentin (Alexa Fluor 488, clone E-5, number sc-373717, Santa Cruz Biotechnology, Dallas, TX) to visualize nuclei morphological features of the HS tissue. Sections were counterstained with SYTO-83 Orange Fluorescent Nucleic Acid Stain (number S11364, Thermo Fisher Scientific) to visualize nuclei.

After staining, HS sections were scanned using a GeoMxTM Digital Spatial Profiler to generate digital fluorescent images. $CD20^+$ B cell regions of interest (ROIs) were preidentified on the basis of CD20 staining of serial sections (see Figure 4f and Supplementary Figure S3b and c), and final ROIs were manually defined from the fluorescent images through the GeoMx profiler.

To cleave the photocleavable oligos from each selected region, UV light was directed through a programmable digital micromirror device, and resultant samples were collected through microcapillary and dispensed into a 96-well plate. Gene expression values for each ROI were quantified by the GeoMx DSP platform. Gene expression values were normalized using the third quartile of all counts from each area of interest and subsequently $\log_2$ transformed before further analysis.

ROI annotation and differential gene expression analysis were done through the GeoMx profiler software (the DE plots in the data report PPT were calculated using the linear mix model with Benjamini–Hochberg correction).

Antibodies for immunohistochemistry

List of antibodies used for Chromogenic Immunohistochemistry and Nanostring (including secondary antibodies) were mouse IgG2aκ anti-human CD20cy (clone L26, M0755, Dako Deutschland, Hamburg, Germany), goat anti-mouse biotinylated (polyclonal antibody, BA-9200, Vector Laboratories, Burlingame, CA), rabbit anti-human CD21 (clone EP3093, ab75985, Abcam), goat anti-rabbit biotinylated (polyclonal antibody, 111-065-144, Jackson ImmunoResearch), monoclonal rabbit isotype control (ab172730,

Abcam), mouse IgG2aκ isotype Control eFluor 660 (50-4724, eBioscience, San Diego, CA), mouse IgG1aκ anti-human pan-cytokeratin Alexa Fluor 647 (clone AE1+AE3, NBP2-33200AF647, Novus Biologicals), mouse IgG2aκ anti-human CD20 Alexa Fluor 594 (clone IGEL/773, number NBP2-47840DL594, Novus Biologicals), and mouse IgG1aκ anti-human vimentin (Alexa Fluor 488, clone E-5, number sc-373717, Santa Cruz Biotechnology).

Image analysis

$CD20^+$ and $CD21^+$ ROIs in chromogenically stained HS skin were identified and outlined manually using the Aperio Imagescope pathology slide viewing software (Leica Microsystems). The association of B cell clusters with fat was assessed and annotated manually. Areas (in μm^2) of $CD20^+$ and $CD21^+$ ROIs were calculated using ImageJ software (National Institutes of Health, Bethesda, MD) and Microsoft Excel.

TNF secretion assay

Monocyte isolation and M1 differentiation. Anonymized buffy coats were received from HVs through the Interregionale Blutspende of the Swiss Red Cross in Bern, Switzerland. The blood was provided under informed consent and collected through the Novartis Tissue Donor Program (TRI0128) in accordance with the Swiss Human Research Act and approval of the responsible ethic committee (Ethikkommission Nordwest- und Zentralschweiz number: 329/13). PBMCs from human peripheral blood were isolated by density gradient centrifugation (Ficoll-Plaque, number 17-1440-03, GE Healthcare) followed by erythrocyte lysis (Buffer EL, number 79217, Qiagen). Human monocytes were then obtained by magnetic isolation (Human Monocyte Isolation Kit, number 19059, Stem Cell Technologies, Vancouver, Canada) according to the manufacturer's instructions. Subsequently, monocytes were cultured for 6 days in RPMI1640 Glutamax (number 72400-021, Gibco, distributed by Thermo Fisher Scientific) supplemented with 10% heat-inactivated fetal bovine serum (number A15-152, PAA laboratories, Toronto, Canada), 1% of sodium pyruvate (number 11360-039, Gibco), 1% penicillin and streptomycin (number 15140, Gibco), 25 mM 4-(2-hydroxyethyl)-1-piperazineethanesulfonic acid buffer (number 15630, Gibco), and 50 μM mercaptoethanol (number 31350-010, Gibco) in the presence of 40 ng/ml colony-stimulating factor 1 (number 216-MC, R&D Systems) and 50 ng/ml IFN-γ (number 285-IF, R&D Systems) at 37 °C and 5% carbon dioxide to differentiate M1 macrophages.

Activation of M1 macrophages with CEL/autoantibody immune complexes. After harvest and wash, M1 macrophages were plated (100K per well at 2×10^6 cells/ml) in a complete RPMI1640 medium without the addition of colony-stimulating factor 1 and IFN-γ in 96-well plates. In parallel, we prepared master mixes of carboxy-methyl-lysine BSA or CEL BSA (number STA-314 and number STA-302, Cell Biolabs, distributed by LubioSciences, Zürich, Switzerland) with either HV or HS sera and incubated for 30 minutes at 37 °C to let the immune complexes form. Whereas HV sera (number S4190-500) were obtained from LabForce (Muttenz, Switzerland), HS sera were obtained from either BioIVT or our internal clinical collaboration. Afterward, 20 μl of the respective master mixture was added to the M1 macrophages (final concentrations for carboxy-methyl-lysine BSA or CEL BSA of 30 μg/ml with HV and HS sera at 1:100) and incubated at 37 °C and 5% carbon dioxide. After 6 hours of incubation, we harvested the supernatants and determined the amount of secreted TNF by homogeneous time-resolved fluorescence (number 62HTNFAPEH, CysBio, Codolet, France).

Quantification and statistical analyses

The statistical details and tests used, the number and representation of n, and any other forms of quantification present are specified in the respective figure legends and results section. All statistical analyses in this study were performed using the Prism 9 software (GraphPad Software).

SUPPLEMENTARY REFERENCES

Gudjonsson JE, Tsoi LC, Ma F, Billi AC, van Straalen KR, Vossen ARJV, et al. Contribution of plasma cells and B cells to hidradenitis suppurativa pathogenesis. JCI Insight 2020;5:e139930.

Lun AT, McCarthy DJ, Marioni JC. A step-by-step workflow for low-level analysis of single-cell RNA-seq data with Bioconductor. F1000Res 2016;5:2122.

Merritt CR, Ong GT, Church SE, Barker K, Danaher P, Geiss G, et al. Multiplex digital spatial profiling of proteins and RNA in fixed tissue. Nat Biotechnol 2020;38:586–99.

Penno CA, Jäger P, Laguerre C, Hasler F, Hofmann A, Gass SK, et al. Lipidomics profiling of hidradenitis suppurativa skin lesions reveals lipoxygenase pathway dysregulation and accumulation of proinflammatory leukotriene B4. J Invest Dermatol 2020;140:2421–32. e10.

Srey C, Hull GL, Connolly L, Elliott CT, del Castillo MD, Ames JM. Effect of inhibitor compounds on N^e-(carboxymethyl)lysine (CML) and N^e-(carboxyethyl)lysine (CEL) formation in model foods. J Agric Food Chem 2010;58:12036–41.

Wickham H. ggplot2: Elegant graphics for data analysis. 2nd ed. New York, NY: Springer International Publishing; 2016.

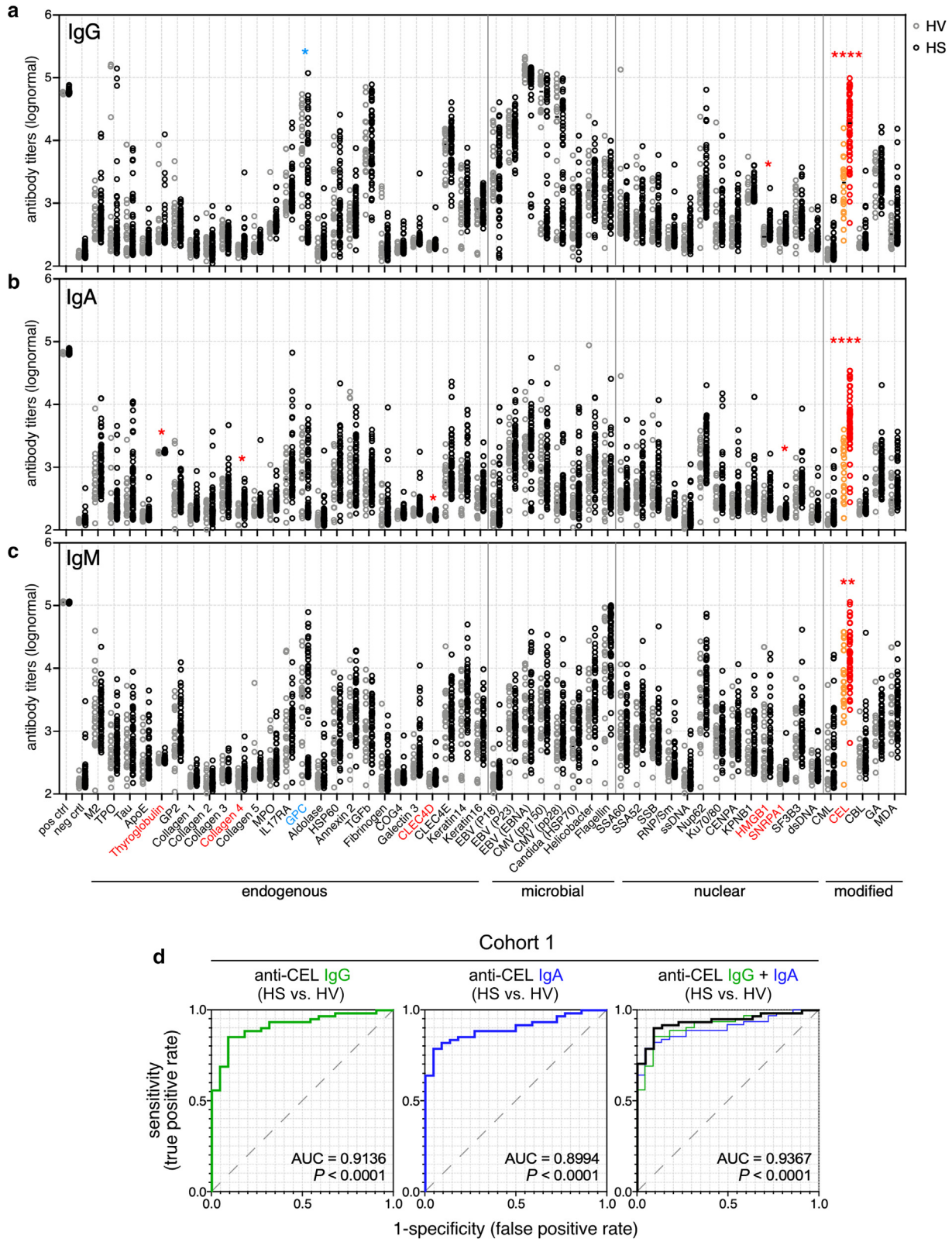

Supplementary Figure S1. Detection of anti-CEL antibodies in patients with HS. (**a**–**c**) Distribution of log-normalized titers of (**a**) IgG, (**b**) IgA, and (**c**) IgM antibodies (arbitrary units) detected in HS sera (n = 61; cohort 1, see Supplementary Table S2) and healthy volunteers (n = 22) targeting the indicated antigens, ordered in five groups: negative/positive controls, endogenous antigens, microbial antigens, nuclear antigens, and post-translational modifications. See Supplementary Table S1 for abbreviations. *$P < 0.05$ and ****$P < 0.0001$ (students *t*-test). Antigens listed in red and blue indicate antigens in which a difference of $P < 0.05$ was observed between the two groups (also indicated by an asterisk). Red indicates higher in HS, and blue indicates higher in healthy volunteers. (**d**) Receiver operator characteristic analysis distinguishing patients with HS (n = 61; cohort 1) from healthy volunteers (n = 22) on the basis of IgG (green, left), IgA (blue, middle), and IgG + IgA (black, right) anti-CEL titers. ApoE, apolipoprotein E; AUC, Area under the curve; CEL, carboxyethyl lysine; dsDNA, double-stranded DNA; EBV, Epstein–Barr virus; GA, glycoaldehyde; HS, hidradenitis suppurativa; HV, healthy volunteers; neg ctrl, negative control; pos ctrl, positive control; ssDNA, single-stranded DNA.

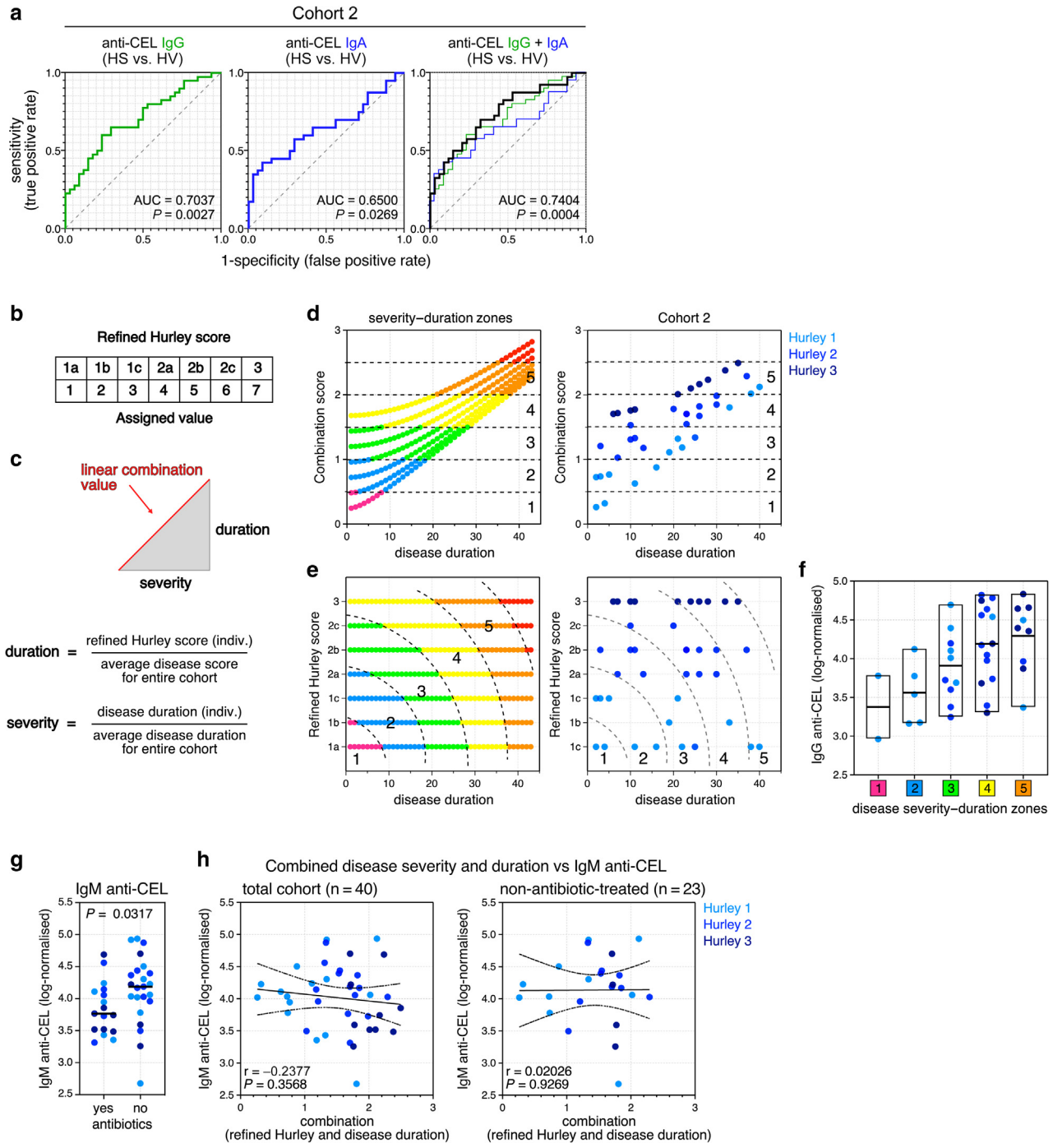

Supplementary Figure S2. Relationship between anti-CEL autoantibodies and clinical parameters in HS. (**a**) Receiver operator characteristic analysis distinguishing patients with HS (n = 40; cohort 2) from healthy volunteers (n = 38) on the basis of IgG (green, left), IgA (blue, middle), and IgG + IgA (black, right) anti-CEL titers. (**b, c**) Calculation of linear combination of severity and duration. (**b**) Refined Hurley scores (1a, 1b, 1c, 2a, 2b, 2c, and 3) were assigned integer values 1–7. Individual values for severity and disease duration (in years) were then normalized against the averages of the entire dataset to equalize the relative contribution of duration and severity. (**c**) Duration–severity combination was calculated using the Pythagorean equation. (**d, e**) Relationship between the combination value, disease duration, and refined Hurley score. Left: All hypothetical values on the left (up to a disease duration of 43 years). Colors indicate linear combination scores of 0–0.5 (zone 1; magenta), 0.5–1.0 (zone 2; blue), 1.5–2.0 (zone 3; green), 2.0–2.5 (zone 4; yellow), 2.5–3.0 (zone 5; orange), and >3.0 (red). Right: Distribution of patient samples (n = 40). (**f**) Log-normalized IgG anti-CEL titers in indicated HS groups. Disease severity–duration zones in **e** and **f** are identical to that shown in Figure 3f. (**g**) Log-normalized distribution of IgM anti-CEL titers in the plasma samples of patients with HS (n = 40; cohort 2), stratified according to whether patients were undergoing treatment with antibiotics (left; n = 17) or not (right; n = 23). $P = 0.0317$ (Man–Whitney U test). (**h**) Scatter plots showing the lack of correlation (Spearman test) between log-normalized IgM anti-CEL titers and the combination of refined Hurley score and disease duration, for the total cohort (left; n = 40) and excluding patients taking antibiotics (right; n = 23). AUC, Area under the curve; CEL, carboxyethyl lysine; HS, hidradenitis suppurativa.

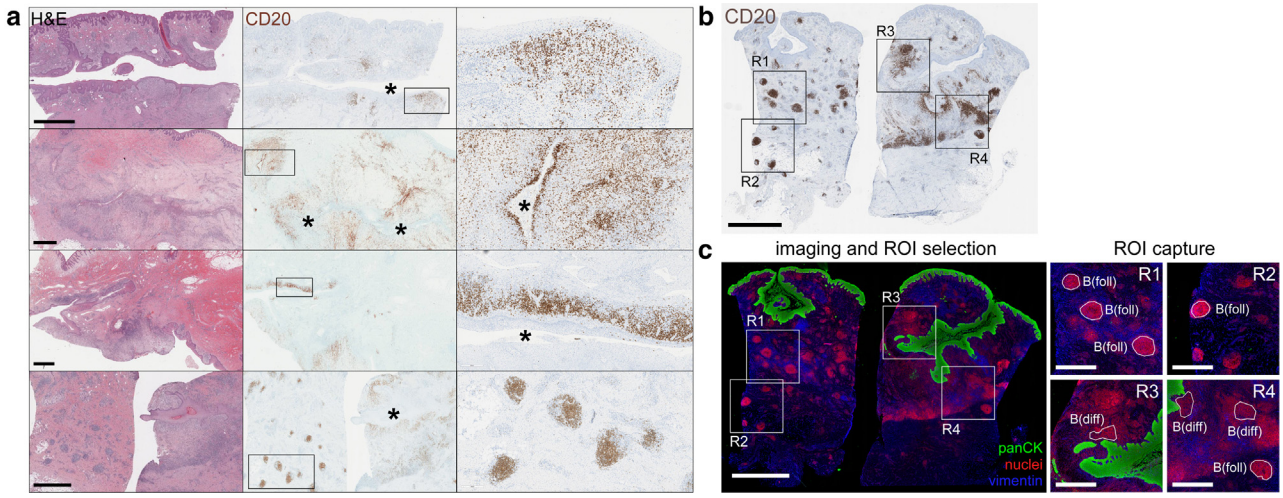

Supplementary Figure S3. Detection and distribution of B cells and germinal center–like structures in HS skin. (**a**) Representative H&E (left) and CD20 staining (middle and right panels) of HS skin samples (n = 4 patients). Boxed regions (middle panels) are shown in higher resolution on the right. Asterisks indicate tunnels. Bars = 2 mm. (**b, c**) Representative staining of (**b**) $CD20^{+}$ B cells and (**c**) immunofluorescence staining of serial sections of patients with HS (bars = 3 mm), identifying B(foll) and B(diff) in four ROIs (R1−R4). Each bar in R1−R4 = 1 mm. The patient sample in **b** and **c** is the same as shown in the bottom panel in **a**. B(diff), diffuse B cell zone; B(foll), B cell cluster; HS, hidradenitis suppurativa; PanCK, pan-cytokeratin; ROI, region of interest.

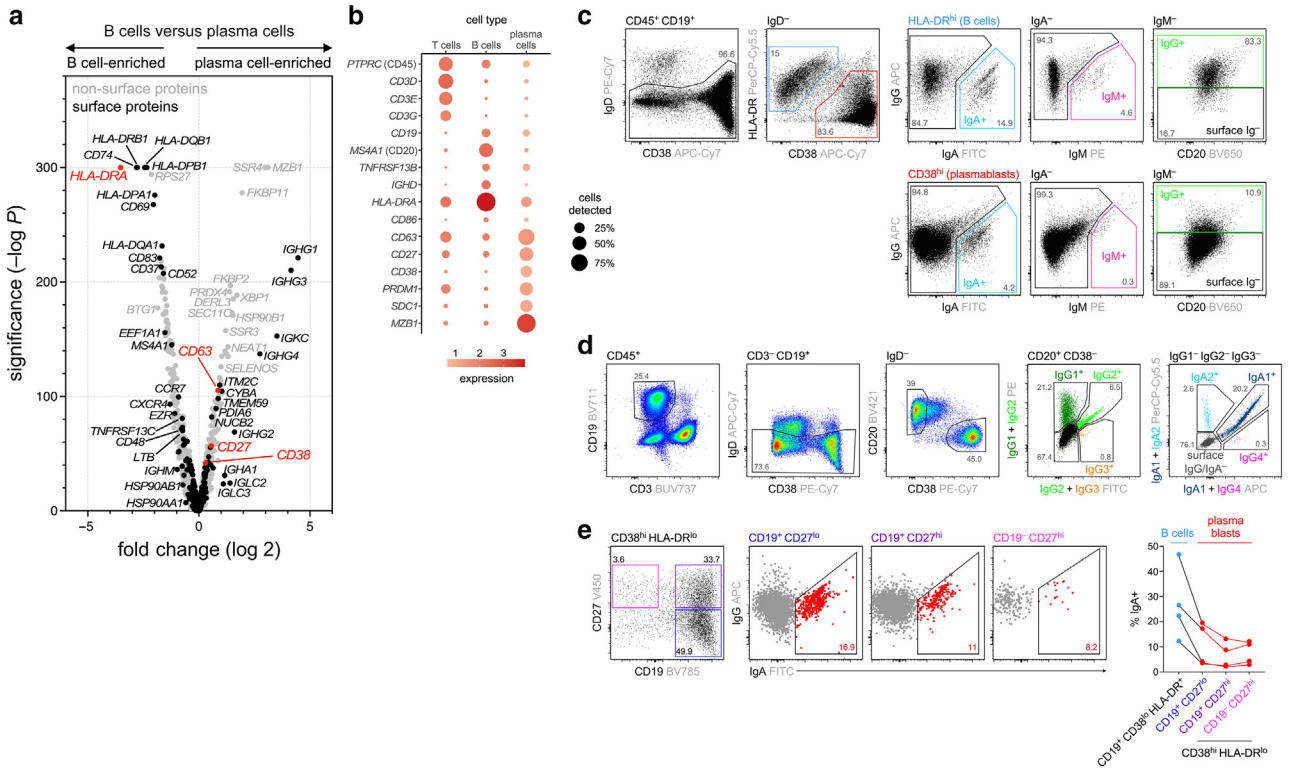

Supplementary Figure S4. Characterization of B cells and plasma cells in HS skin. (**a**) Comparison of gene expression in B cells versus in plasma cells by volcano plot from single-cell RNA-sequencing data of HS lesional skin (Gudjonsson et al., 2020). Genes encoding proteins expressed on the cell surface are marked in black. Selected genes encoding cell surface proteins used in flow cytometry experiments in this study are marked in red. (**b**) Dot plots of pooled T-, B-, and plasma cell clusters in single-cell RNA-sequencing data of HS lesional skin (Gudjonsson et al., 2020), displaying the average gene expression (red intensity) and frequency of positive cells (circle size) of indicated markers. (**c, d**) Representative flow cytometry dotplots showing the gating strategy for identifying Ig isotypes (**c**) and subclasses (**d**) on the surface of CD20^{hi} HLA-DR^{+} CD38^{lo} B cells and CD20^{lo} HLA-DR^{lo} CD38^{hi} plasmablasts in lesional HS skin. (**e**) Left: Representative flow cytometry dotplots depicting surface IgA expression by indicated subpopulations of HLA-DR^{lo} CD38^{hi} plasmablasts isolated from lesional HS skin. Right: Frequency of surface IgA^{+} B cells (blue) and indicated subpopulations of HLA-DR^{lo} CD38^{hi} plasmablasts (red) isolated from lesional HS skin (n = 4). HS, hidradenitis suppurativa.

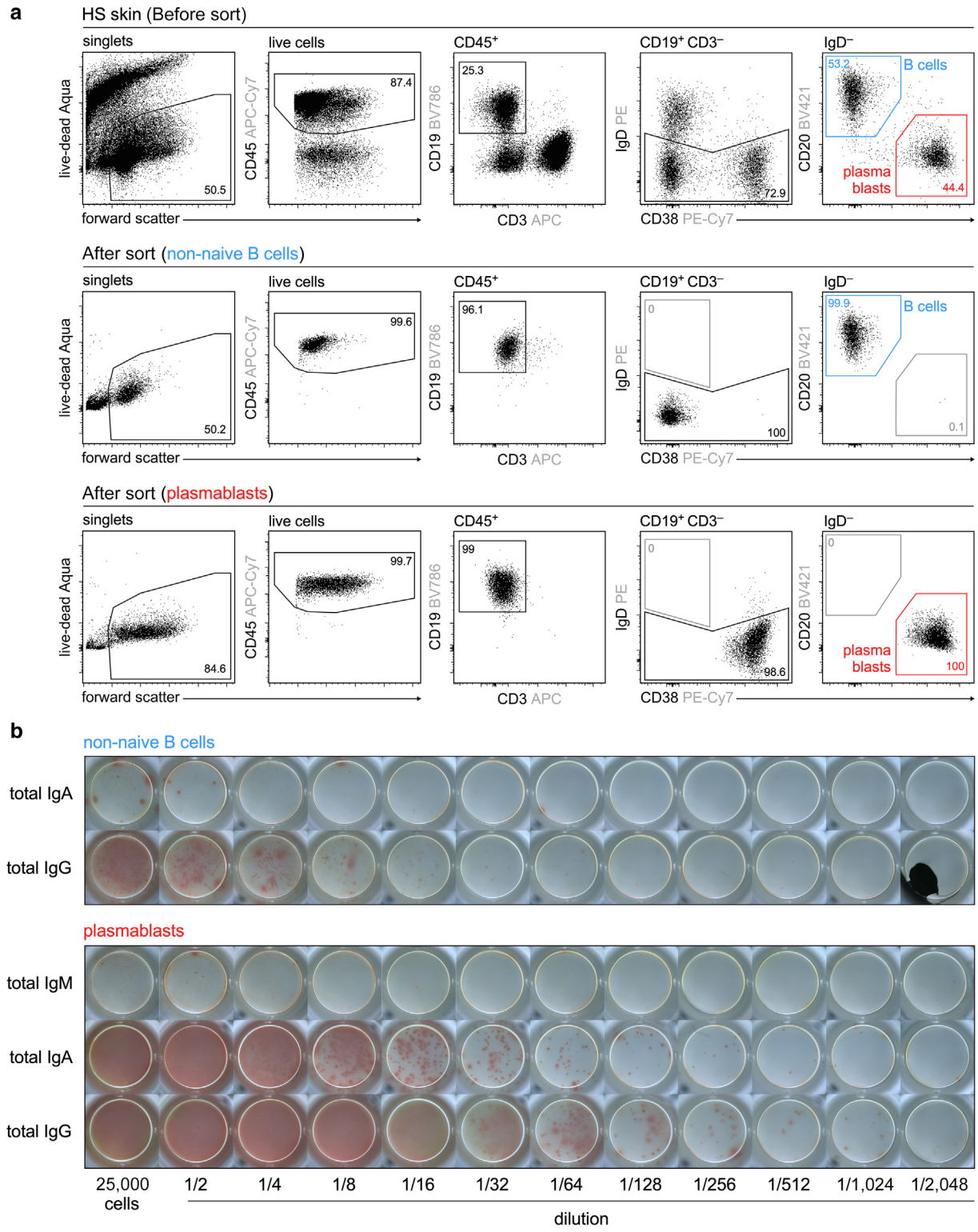

Supplementary Figure S5. ELISPOTs of sorted B cells and plasmablasts from HS skin. (**a**) Representative flow cytometry dotplots showing the gating strategy for identifying (non-naïve) CD20^{hi} CD38^{lo} B cells (blue box) and CD20^{lo} CD38^{hi} plasmablasts (red box) in lesional HS skin before (top panel) and after (bottom two panels) sorting for ELISPOT readouts. (**b**) Representative ELISPOT plates of B cells (top) and plasmablasts (bottom) sorted from HS skin, identifying the presence of (total) IgA and IgG antibody-secreting cells. Data are representative of three independent experiments and show a dilution series, starting from 2.5×10^4 cells per well. ELISPOT, enzyme-linked immunosorbent spot; HS, hidradenitis suppurativa.

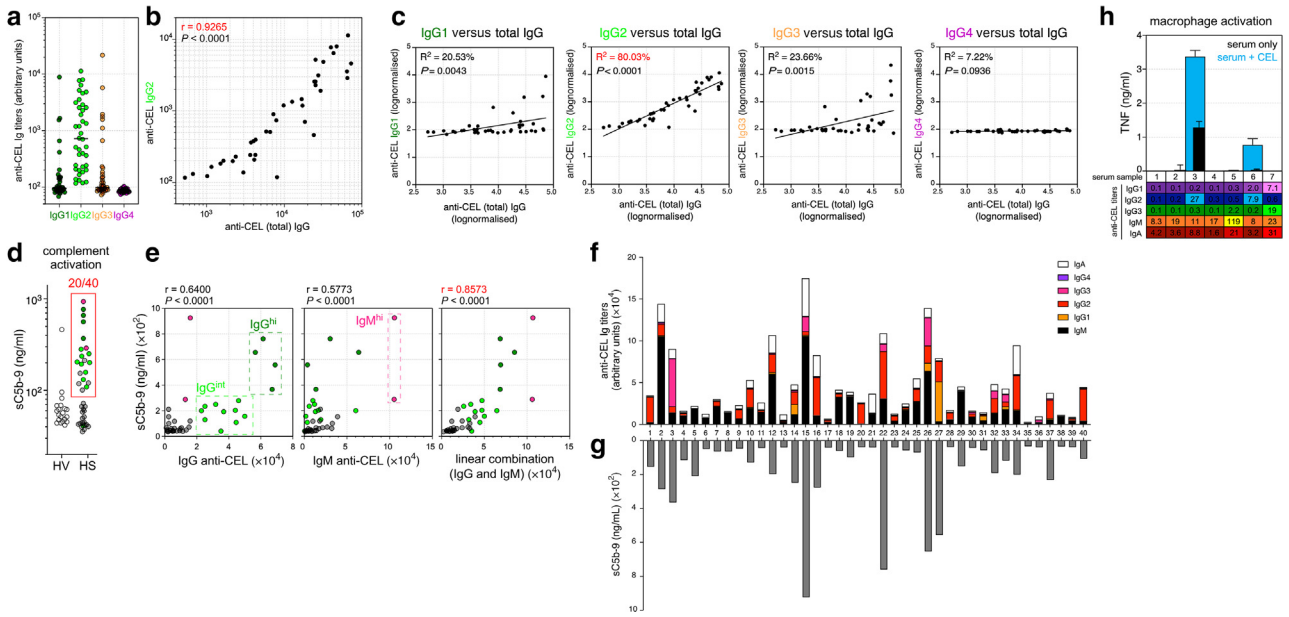

Supplementary Figure S6. Isotype and functional capabilities of anti-CEL autoantibodies in patients with HS. (**a**) Log distribution of IgG1, IgG2, IgG3, and IgG4 anti-CEL titers in HS plasma samples (n = 40; cohort 2). (**b**) Scatter plot depicting the correlation between total IgG anti-CEL and IgG2 anti-CEL in HS plasma samples from cohort 2 (n = 40). $P < 0.0001$ (Spearman test). (**c**) Linear regression analyses of log normalized (total) IgG anti-CEL versus IgG1, IgG2, IgG3, and IgG4 anti-CEL titers in the cohort 2 HS plasma samples (n = 40). (**d**) Detection of sC5b-9 complex in the plasma of HVs (n = 20) and patients with HS (n = 40) after 1-h incubation in CEL BSA–coated plates in the presence of excessive complement from healthy serum. (**e**) Scatter plots depicting the correlation between sC5b-9 and IgG (left), IgM (middle), and IgG + IgM (right) anti-CEL titers in HS plasma samples (n = 40) (Spearman test). Individual samples have been colored on the basis of whether they exhibited high anti-CEL IgM (pink) or IgG (green) titers. (**f**) Cumulative abundance of IgM, IgA, IgG1, IgG2, IgG3, and IgG4 anti-CEL titers within the plasma of individual patients with HS (HS1–HS40). (**g**) Detection of sC5b-9 complex in plasma from indicated patients with HS (n = 40) after 1-h incubation in CEL BSA–coated plates in the presence of excessive complement from healthy serum. (**h**) TNF secretion by in vitro generated macrophages 6 h after incubation with commercially obtained serum from patients with HS (n = 7) in the presence (blue bars) or absence (black bars) of CEL BSA. Titers of indicated Ig isotypes and subclasses of anti-CEL (arbitrary units [$\times 10^2$]) in each of the seven serum samples are indicated in the bottom panel. CEL, carboxyethyl lysine; h, hour; HS, hidradenitis suppurativa; HV, healthy volunteer; sC5b-9, soluble complement 5b-9.